Master Thesis

A primary applicability study of terrestrial laser scanning on engineering rock mass characterization

Graz University of Technology

Institute of Applied Geosciences

Author:

Britta Larsen

Advisor:

Ao.Univ.-Prof. Mag.rer.nat. Dr.rer.nat Qian LIU

Graz, March 2012

Erklärung

Ich erkläre an Eides statt, dass ich die vorliegende Arbeit selbstständig verfasst, andere als die angegebenen Quellen/Hilfsmittel nicht benutzt, und die den benutzten Quellen wörtlich und inhaltlich entnommene Stellen als solche kenntlich gemacht habe.

Graz, am …… ……..

(Unterschrift)

Acknowledgements

First of all I want to thank my supervisor Ao, Univ.-Prof.Mag.Dr. Qian Liu for his support and the many hours patiently giving me advice. I could always knock at his door and ask questions, no matter how busy he was.
Next I want to express my deepest gratitude to my parents Elsa and Kjeld Larsen without whom I would not have been able to complete my studies. Though they had to be very patient sometimes, they always supported me both financially and mentally and believed in my success. I want to thank my brother Lars for advising me how to work on a project like a Master Thesis.
Special thanks go to my mother and Mr. Andrew Turner who helped me correcting my Thesis in terms of spelling mistakes, English grammar and expression.
Furthermore I want to thank my dear colleagues and friends, Elisabeth Macher, Maike Schäbitz, Markus Kaspar, Luiz Felipe Rocha and Christoph Steinbauer for all the “motivation coffees” and supportive talks and discussions.
I also want to thank the staff of the institute: Anna Pendl for keeping everything organized, Peter Schreiber for helping with hardware and software problems and Gerhard Lauk for explaining the most important details of the laser scanner to me.
Last but not least I want to thank “Brüder Rath Steinbrüche Ges.m.b.H.” and the community of Arzberg for giving us the opportunity to scan the quarry in Angenofen and the gallery of Arzberg and by this gave me the possibility to work on an interesting subject for my Master Thesis.

Zusammenfassung

Diese Arbeit gibt einen Einblick in terrestrisches Laser-Scannen in der Ingenieurgeologie. Die Vorteile solcher Aufnahmen gegenüber herkömmlichen Methoden sind u.a. schnelle Erfassung von großen Gebieten, die nicht oder nur unter großem Risiko zu erreichen sind, und ein naturgetreues 3D-Modell mit sehr hoher Genauigkeit. Abhängig von der Verwendung eines GPS kann dieses Modell auch geo- referenziert sein. In jedem Fall können für die Ingenieurgeologie wichtige Orientierungsangaben gemacht werden, da die Daten gegen Norden referenziert werden können.

Weiters beschäftigt sich diese Arbeit mit der Methodik der Messung wichtiger ingenieurgeologischer Parameter wie beispielsweise Orientierung von Flächen, Trennflächenabstand und Rauhigkeit mit RiSCAN PRO.

Zur Bestimmung der Genauigkeit der Orientierungsmessungen wurden die mit RiSCAN PRO erzielten Ergebnisse mit einem bereits erprobten Programm, welches auf digitaler Photogrammetrie (ShapeMetrix^{3D}) basiert, und mit Kompassmessungen verglichen.

Abstract

This thesis deals with the application of terrestrial laser scanning in engineering geology. Advantages of laser scan data are a rapid collection of data in a comparatively short time, data acquisition of outcrops which are not accessible without risk for the investigators and a photo-realistic accurate 3D-model of the scanned outcrop. If a RTK-GPS was used this model can also be georeferenced. In either case orientations can be measured since the collected data can be referenced to north.

Furthermore this thesis deals with the methodology of measuring important parameters for rock mass characterization like orientation, spacing and roughness of discontinuities.

To determine the accuracy of orientation measurements made by RiSCAN PRO, the results were compared to a more tested photogrammetric program (ShapeMetrix^{3D}) and compass measurements.

Contents

1 Introduction

In engineering geology rock mass characterization is important to provide safe conditions during and after construction. Investigators often face the problem how to reach the outcrop without risking their own lives. As time is money the sampling and characterization of a usually large area must be fast and accurate but also statistically representative and objective. The development of photogrammetry improved the situation for investigators, but in case of rather large outcrops with huge vertical extension it still might be too time consuming to cover the whole outcrop. Therefore a tendency to rock mass characterization using rapid remote sensing methods with high resolution could be observed.

In the past few years terrestrial laser scanning has been tested as a surveying method in engineering geology (e.g. Liu & Kieffer, 2011). The long range of the equipment enables detailed remote sensing of large outcrops that are usually not accessible. The scanner provides 3D data information of every collected point. Combined with a camera and a RTK-GPS receiver that are mounted on the scanner the result of a scan is a colored georeferenced 3D-point cloud with high resolution. Due to the high point density, nowadays parameters for rock mass characterization such as orientations are also determined by using the point cloud. For detailed determination of e.g. trace length, termination and roughness a georeferenced, photo-realistic 3D-model is created out of the point cloud.

The aim of this thesis is to introduce measurement methods for parameters that are important for rock mass characterization by using the program RiSCAN PRO, the program available to process laser scan data at TU Graz.

2 Basics

2.1 Introduction to LiDAR

Basically LiDAR (Light Detection and Ranging), also called laser scanning, uses the ability of objects to reflect light. Since the laser scanner has its own coordinate system (Figure 1) for each point which is scanned 3D-coordinates are collected. The result is a detailed 3D point cloud of the scanned outcrop (Chapter 3.4.5).

Depending on the field of application, nowadays equipments are available for the accomplishment of airborne and terrestrial laser scanning. Though in this thesis only a terrestrial laser scanner was used, airborne laser scanning will also be described.

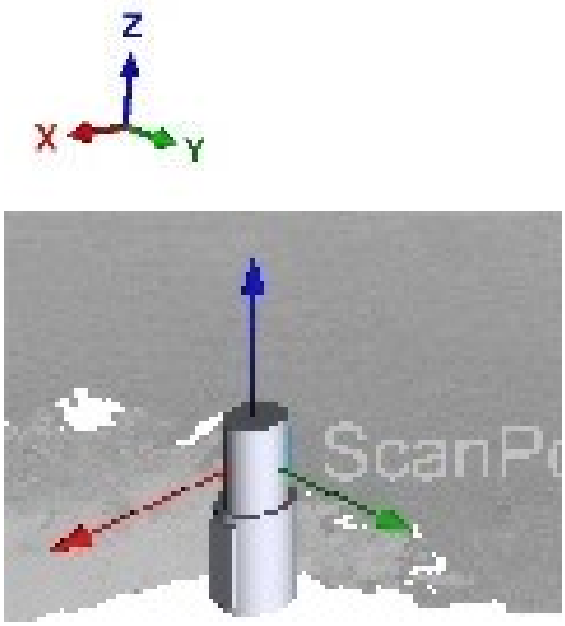

Figure 1

2.1.1 Airborne LiDAR

Airborne LiDAR is performed with the scanner installed on a plane or helicopter and is also called airborne laser scanning (ALS).
The exploration area is flown across in overlapping horseshoe bends. The sampling density is several points per square meter. Depending on the equipment the flight altitude can vary from 100 to 6000 m (Hyyppä et al in The SAGE Handbook of Remote Sensing, 2009)
“Since it is a priori not known which targets generated the echoes, models are required for converting the 3D point cloud into geospatial data products such as Digital Terrain Models (DTM) […]” (Hyyppä et al in The SAGE Handbook of Remote Sensing, 2009, p.199).
Airborne LiDAR is most favored for gathering surface information for e.g. topography, agricultural use and locations of historical villages for archaeologic purposes. For engineering geology airborne LiDAR might be useful for the approach to geomorphic landforms such as landslides or drainage systems (Hyyppä et al in The SAGE Handbook of Remote Sensing, 2009).

2.1.2 Terrestrial Laser Scanning

In terrestrial laser scanning two types of laser scanners are applied:

- Phase-shift laser scanners
- Time-based laser scanners

They differ in measuring principle but also in range and accuracy.

Phase-shift laser scanners emit a beam “with sinusoidally modulated optical power” (Kemeny et al 2008, p. 3). When the wave is reflected by the rock mass a phase shift appears which is measured by the scanner. The time of flight is determined with Equation 1:

$$Time\ of\ Flight = \frac{Phase\ Shift}{(2\pi \cdot Modulation\ Frequency)}$$

(Kemeny, 2008) **Equation 1**

With the current time known the distance between the rock mass and the scanner is calculated with Equation 2:

$$Distance = \frac{(Speed\ of\ Light \times Time\ of\ Flight)}{2}$$

(Kemeny, 2008) **Equation 2**

The maximum range of phase-shift laser scanners is 80 m and the accuracy is 25 mm (Slob, 2010).

Time-based laser scanners emit a light impulse. Then the time of flight of the pulse is measured. When the velocity of light and the time of flight are known, the distance to the rock can be calculated using Equation 2.
The scanner used in this thesis has a maximum range of 2000 m and an accuracy of 10 mm (Link 4).
Time-based laser scanners are more favorable for engineering geology applications because of larger range and higher accuracy.

2.1.2.1 Advantages of Terrestrial Laser Scanning

Terrestrial laser scanners collect a large number of data in a comparatively short time which results in more representative samples for statistical analysis. The resulting point cloud is a permanent, georeferenced record with high accuracy and offers 3D-information of

the scanned area. With the photos that are taken of each scan position a photo-realistic model of the surface is created. Due to the range of the scanner an increase of safety for the investigators is achieved because data of inaccessible and dangerous outcrops can be collected without even getting near the rock mass (Sturzenegger, 2009).
Since LiDAR is an active surveying method which emits light impulses it is independent of natural light conditions at the outcrop and good results can be achieved under poor light conditions.

2.1.2.2 Applications of Terrestrial Laser Scanning

Terrestrial laser scanning is used in a wide field of geology and geomorphology because of its advantages. The high resolution of a point cloud is used to determine small changes of volume and slope angles in the mining industry (Link 1) as well as for rock mass characterization and discontinuity analysis in engineering geology (Slob,2010).
In 2004 Abellán, Vilaplana and Martínez investigated the rock fall of Vall de Núria in Spain with a terrestrial laser scanner, created a DEM out of the point cloud and calculated, amongst others the volume and trajectories of the rocks.
Multi-temporal scans were performed by Schwalbe et al 2007 in Greenland for determination of glacier tongue velocity and generation of a model of glacier height. Another multi-temporal scan survey was performed by Bitelli, Dubini and Zanutta to generate a detailed digital surface model of the Cà di Malta landslide in Italy.
Further fields of application are the survey of coastal erosion (Penington and Holls, 2008), city modeling, architecture and archaeology (Link 2). Recently a Riegl LMS-Z420i was installed permanently to observe the movements of the ship wreck of Costa Concordia inshore of the Italian island Giglio (Link 3).

2.2 Discontinuity Characterization

To avoid rock failure or mass movements a detailed characterization of the rock mass, especially discontinuities, is needed. Parameters like permeability and rock strength are highly influenced by discontinuity properties. Thus a proper discontinuity characterization should be accomplished. For data collection in the field usually a scanline or photogrammetric approach (Chapter 3.2) is used.

2.2.1 Scanline

A scanline is a measuring tape of 2-30 m of length which is pinned to the outcrop in strike direction. Data of all discontinuities along the measuring tape and the plunge and trend of the scanline are collected (Priest, 1993). Priest (1993) recommends that both start and endpoint of a scanline are intersection points of discontinuities.
Following data is collected for each discontinuity along the scanline (Priest, 1993):

- Intersection distance [m]
- Orientation (Dip/Dip direction in degrees)
- Semi-trace length above (left) or below (right) of the scanline
- Termination
- Roughness
- Curvature

Additionally also parameters like weathering, aperture, filling, wetness, friction angle and UCS can be estimated (ISRM, 1981).

2.2.2 Discontinuity Orientation

Given by dip angle and dip direction (Figure 2a), Priest (1993) believes the orientation to be the most important parameter for discontinuity

description. Both, the orientation to the engineering project but also the orientation of two discontinuities to each other, can influence the rock mass behavior in terms of permeability, rock strength and failure modes like toppling, plane sliding and wedge sliding (Priest, 1993).

“The importance of orientation increases when other conditions for deformations are present, such as low shear strength and a sufficient number of discontinuities or joint sets for slip to occur.” (ISRM, 1981, p. 6) Joint planes can be illustrated two-dimensionally in an equal area stereonet by plotting them in great circles or by their poles (Figure 2b).

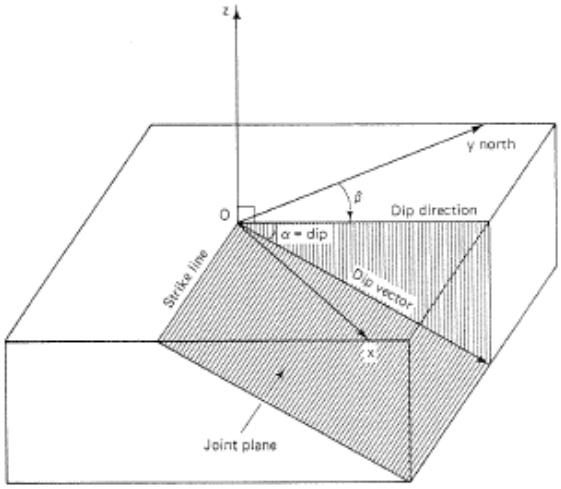

a)

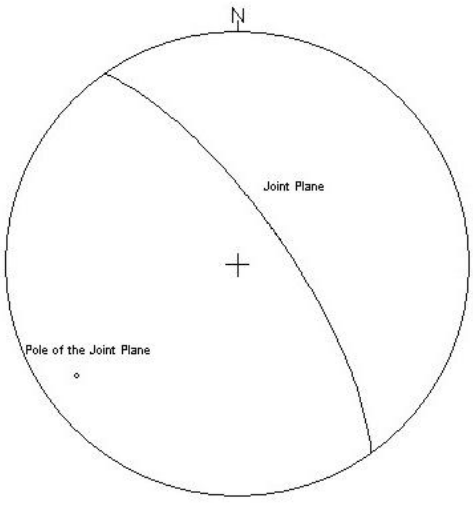

b)

Figure 2: Definition of dip angle and dip direction (a) (Goodman, 1985), and plotting of orientations on the right side (b)

Depending on their orientations different joint sets can be defined. These affect both the ability of deformation before intact rock failure and the overbreak when the excavation is performed by blasting (ISRM, 1981).
Controlled by the number and filling of joint sets a rock mass can be characterized from massive to crushed and earth like rock (ISRM, 1981) .

2.2.3 Discontinuity Spacing

The block size of a rock mass depends on the spacing of adjacent discontinuities. Close discontinuities cause small blocks and thus low mass cohesion whereas wide spaced discontinuities assure high mass cohesion (ISRM, 1981). “In exceptional cases a close spacing may change the mode of failure of a rock mass from translational to circular […].” (ISRM,1981, p. 17)
Furthermore spacing has high influence on permeability and its importance increases in combination with low shear strength (ISRM, 1981).
The common way of determination of true spacing is described below.
Figure 3 shows the relation between apparent spacing (AP) which is measured along the scanline and true spacing (R) which is the normal of the discontinuity. AP and R form θ.

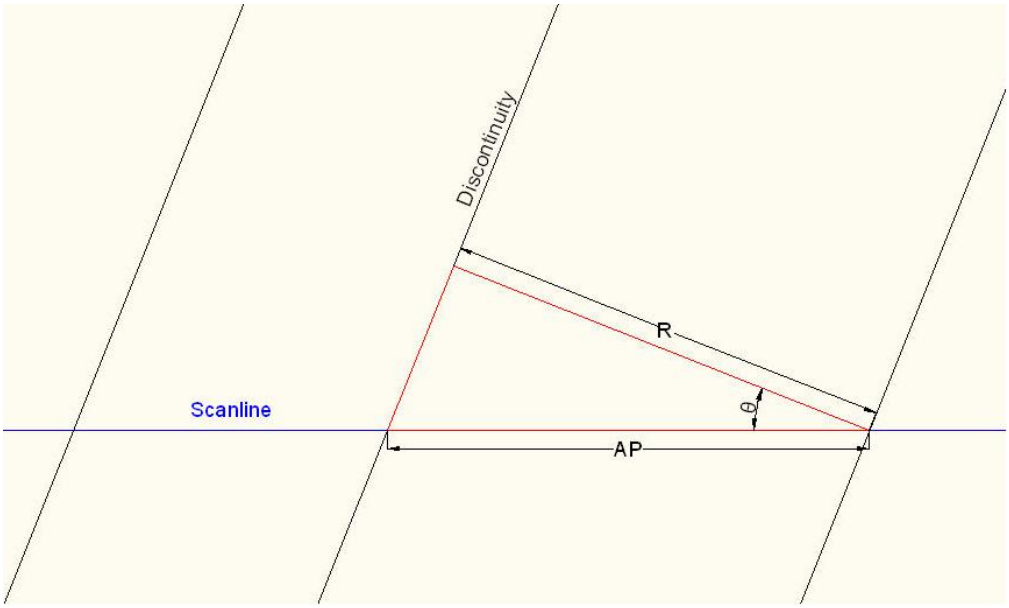

Figure 3: Relation between apparent spacing and true spacing

θ can be determined if the orientations of the scanline and of the discontinuity plane are known. θ is the smallest angle between the pole of the discontinuity and the vector representing the scanline (plunge/plunge direction of the line) (Figure 3).

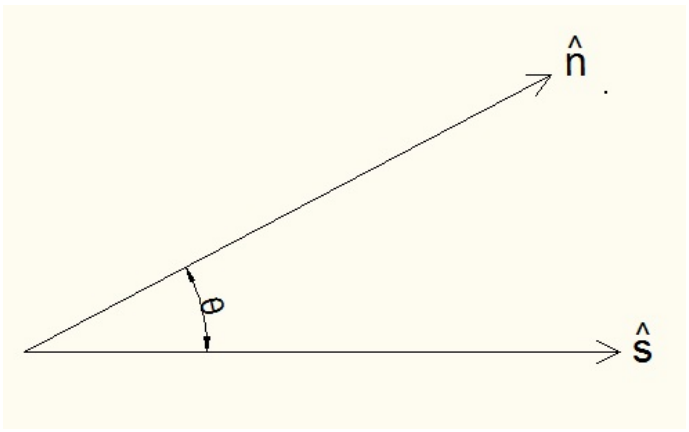

Figure 4

Figure 4 shows the vectors for the discontinuity pole (n) and the scanline (s). For calculation of θ the dot product is applied (Equation 3).

$$\theta = arcos(\frac{\hat{n} \cdot \hat{s}}{|\hat{n}| \cdot |\hat{s}|})$$

Equation 3

For calculation of the true spacing (R) Equation 4 which results out of Figure 3 is used.

$$\cos\theta = \frac{R}{AP}$$

$$R = AP \cdot \cos\theta$$

Equation 4

Classification for spacing according to ISRM 1981 is given in Table 1:

Description	Spacing [mm]
Extremely close spacing	< 20
Very close spacing	20 – 60
Close spacing	60 – 200
Moderate spacing	200 – 600
Wide spacing	600 – 2000
Very wide spacing	2000 – 6000
Extremely wide spacing	> 6000

Table 1: Definitions for spacing (ISRM, 1981)

2.2.4 Frequency

Frequency is the number of discontinuities per volumetric, areal or linear unit. Depending on the mode of data acquisition the volumetric, areal or linear frequency can be calculated. Linear frequency is the most common calculated one, as it is the reciprocal value of the true spacing (Priest, 1993).

For determination of areal frequency the central points of the discontinuity trace are counted per areal unit whereas for volumetric frequency it is assumed that discontinuities are represented by their centroids (Priest, 1993). It is defined as the “average number of these points per unit volume of rock sample” (Priest, 1993, p. 93).

2.2.5 Block Size

Influenced by persistence, spacing and number of discontinuity sets, block size is an important factor for rock mass behavior.

Large blocks tend to form interlocking modes whereas small blocks can influence the failure mode of a slope (ISRM, 1981). “In exceptional cases ‘block’ size may be so small that flow occurs (ISRM, 1981, p. 45).”
Furthermore spacing and number of discontinuity sets do not only influence the size but also the shape of the block which may be important for key block theory.
“Block size can be described either by means of the average dimension of typical blocks (block size index I_b), or by the total number of joints intersecting a unit volume of the rock mass (volumetric joint count J_v) (ISRM, 1981, p. 45).” The J_v is the number of discontinuities of a joint set that occur per meter. ISRM suggests a sampling length of 5 or 10 meters. Depending on the J_v a rock mass can be described with terms mentioned in Table 2.

Description	J_v (joints/m³)
Very large blocks	< 1.0
Large blocks	1 – 3
Medium – sized blocks	3 – 10
Small blocks	10 – 30
Very small blocks	> 30

Table 2: Terms for volumetric joint count after ISRM, 1981.

2.2.6 Trace Length and Termination

Traces can either be recorded in their full length or as semi-trace length. Latter is the distance between the intersection point with the scanline and the end of the trace (Priest, 1993).
Along with trace lengths termination often is recorded. It is important for estimation of persistence. Discontinuity traces either end in intact rock (R), in another discontinuity (D) or the end cannot be clearly defined in the observed outcrop (X). For presentation of termination the so-called termination index (T_r) was developed (ISRM, 1981). “T_r is defined as the

percentage of discontinuity ends terminating in rock compared to the total number of terminations (ISRM, 1981, p. 21).” (Equation 5)

$$Tr = \frac{\sum R \cdot 100}{2 \cdot (\sum R + \sum D + \sum X)} \%$$

Equation 5

(ISRM, 1981)

If only semi-traces were recorded in a scanline Equation 6 may be applied (Priest, 1993).

$$Tr = \frac{\sum R \cdot 100}{(\sum R + \sum D + \sum X)} \%$$

Equation 6

(after Priest, 1993)

2.2.7 Roughness

Joint roughness can be subdivided into large scale waviness for discontinuities larger than one meter and small scale smoothness for joints smaller than one meter (Palmström, 2001). The small scale smoothness affects the shear strength whereas waviness may influence direction of the shear that might occur (ISRM, 1981).

The most common method for determination of roughness is the comparison of the recorded joints to typical joint roughness and joint waviness profiles introduced by Barton 1976 (Figure 5 a & b). It also allows estimation for JRC (Joint Roughness Coefficient).

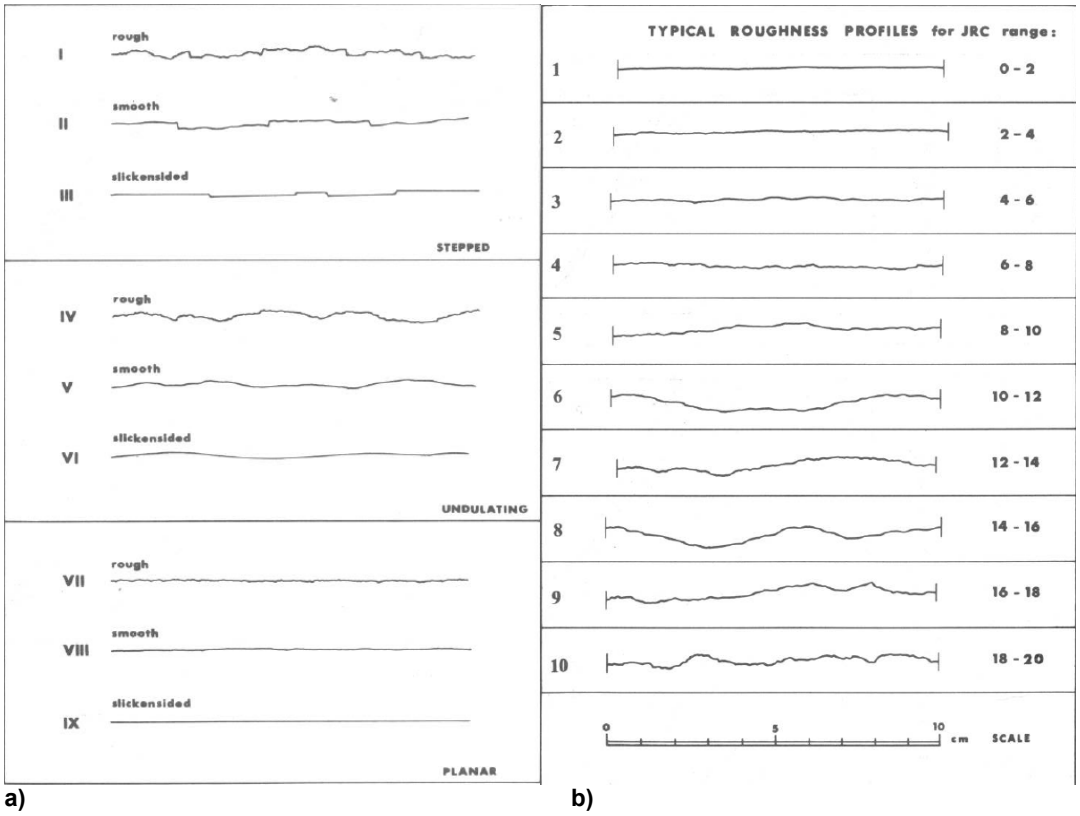

Figure 5: Waviness (a) and small scale roughness (b) profiles after Barton (ISRM, 1981).

Another more mathematical approach was introduced by Palmström 1995. Lengths and maximal amplitudes of discontinuity surfaces are collected in the field (Figure 6).

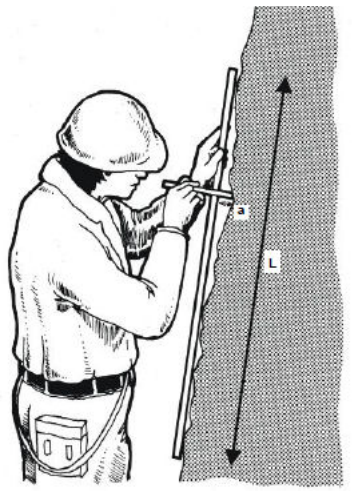

Figure 6: Determination of Length (L) and amplitude (a) in the field (Palmström, 2001).

Then the undulation (%) for a joint surface is calculated with Equation 7:

$$Undulation = \frac{Amplitude\ (a)}{Measured\ Length\ (L)}$$

Equation 7

Palmström (2001)

By comparison of the results of undulation with Figure 7 a division from smooth to very rough for smoothness and from planar to strongly undulating for waviness can be made.

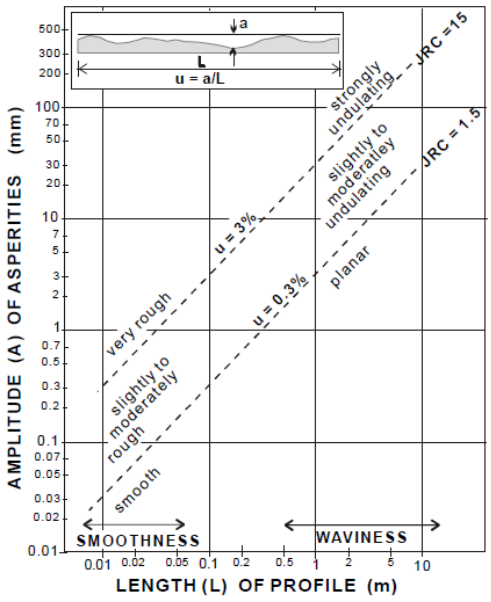

Figure 7: Dependence of smoothness and roughness on discontinuity length and amplitude (Palmström, 2001).

In terms of waviness the undulation (u) can be expressed as joint waviness factor (j_w) (Table 3).

TERM	Undulation (u = a/L)	Waviness factor (jw)
Interlocking (large scale)		3
Stepped		2.5
Large undulation	u > 3 %	2
Small undulation	u = 0.3 - 3 %	1.5
Planar	u < 0.3 %	1

Table 3: Determination of the waviness factor (Palmström, 2001).

Another way of estimation of smoothness, described by Palmström (2001), is touching the rock by hand. Then a smoothness factor (j_s) can be determined (Table 4).

TERM	DESCRIPTION	Smoothness factor, js
Very rough	Near vertical steps and ridges occur with interlocking effect on the joint surface.	3
Rough	Some ridge and side-angle steps are evident; asperities are clearly visible; discontinuity surface feels very abrasive. (like sandpaper grade approx.< 30)	2
Slightly rough	Asperities on the discontinuity surfaces are distinguishable and can be felt. (like sandpaper grade approx. 30 - 300).	1.5
Smooth	Surface appear smooth and feels so to the touch. (smoother than sandpaper grade approx. 300).	1
Polished	Visual evidence of polishing exists, or very smooth surface as is often seen in coatings of chlorite and specially talc.	0.75
Slickensided	Polished and often striated surface that results from friction along a fault surface or other movement surface.	0.6 - 1.5

Table 4: Determination of the factor for smoothness (Palmström, 2001)

A joint roughness factor results from multiplication of j_w and j_s (Table 5) (Palmström, 2001).

(The ratings in *bold italic* are used for Jr in the Q system)		Large scale waviness of joint plane				
		Planar	Slightly undulating	Undulating	Strongly undulating	Stepped or interlocking
Small scale smoothness of joint surface	Very rough	2	3	4	6	6
	Rough	***1.5***	2	***3***	4.5	6
	Smooth	***1***	1.5	***2***	3	4
	Polished or slickensided *)	***0.5***	1	***1.5***	2	3
	For filled joints jR = 1 For irregular joints a rating of jR = 6 is suggested					
*) *For slickensided surfaces the ratings apply to possible movement along the lineations*						

Table 5: Determination of the roughness factor (Palmström, 2001).

However, as this method is rather subjective the measurement of length and maximal amplitude is more recommended.

3 Methodology

3.1 Riegl LMS Z620

The data in this thesis was recorded with the RIEGL LMS-Z620 (Figure 8a). This is a time-based class 1 laser scanner with a maximum range of 2000 m, an accuracy of 10 mm and a precision of 5 mm (Link 4).
Horizontally a full 360° scan can be performed. The maximal vertical field of view is 80° (Figure 8b) (Link 4). To increase the vertical scanning range the scanner has a mount for manual tilt with a tilt range of +/- 90 ° (Figure 8c) (Link 5). Additionally a RTK-GPS and a camera can be mounted on the scanner.

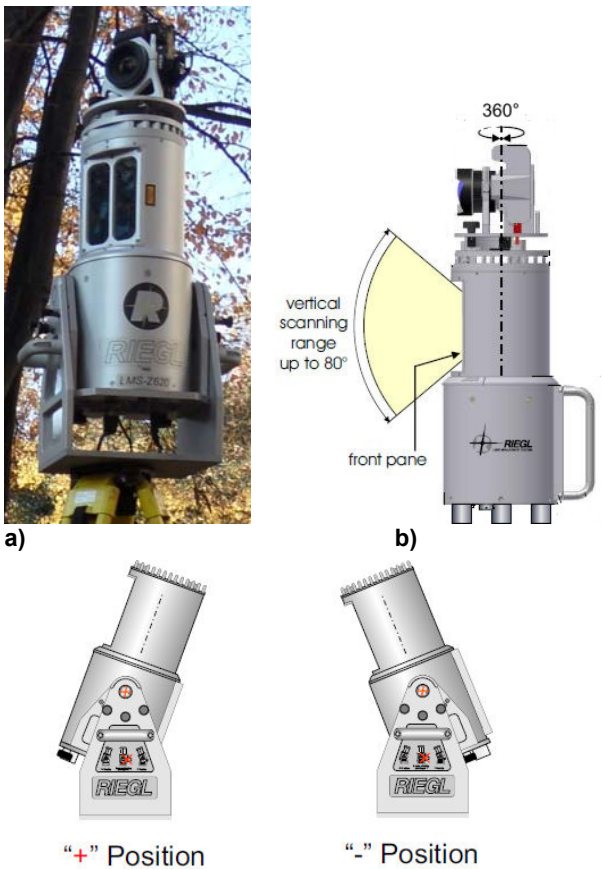

Figure 8: a) The RIEGL LMS Z620 (with camera mounted) has a (b) vertical scanning range of 80° (modified after an image of Link 4). c) Tilting of the scanner increases the vertical range (image from Link 5).

Data post processing was accomplished with RiSCAN PRO, the software for data recorded with RIEGL laser scanners.

3.2 ShapeMetrix^{3D}

ShapeMetriX^{3D} was used for verification of the orientation measurements of LiDAR. This program is based on digital photogrammetry.

For data acquisition two overlapping photographs are taken of the site from different positions (stereoscopic image pair). Reference targets are installed at the site and must be visible on both photos. One target is a so-called range pole which consists of two disks that are vertically fixed on a bracket. Since the distance between these targets is known the range pole can be used for scaling. From the range pole the direction to another target is measured with a compass to define the orientation. After scaling and referencing the images with the SMX Normalizer, using the reference targets, a 3D metric image is created with the SMX Reconstructor. Figure 9 shows the principle for generation of a 3D point out of the two images taken at the site (ShapeMetriX^{3D} Manual, 2006). "From the determined orientation between the two images and a pair of corresponding image points P(u, v) imaging rays (red) are reconstructed whose intersection lead to a 3D surface point P(X, Y, Z). This procedure is repeated for a dense grid of measuring points which are connected then to 3D surface model" (ShapeMetriX^{3D} Manual, 2006, p. 2-3).

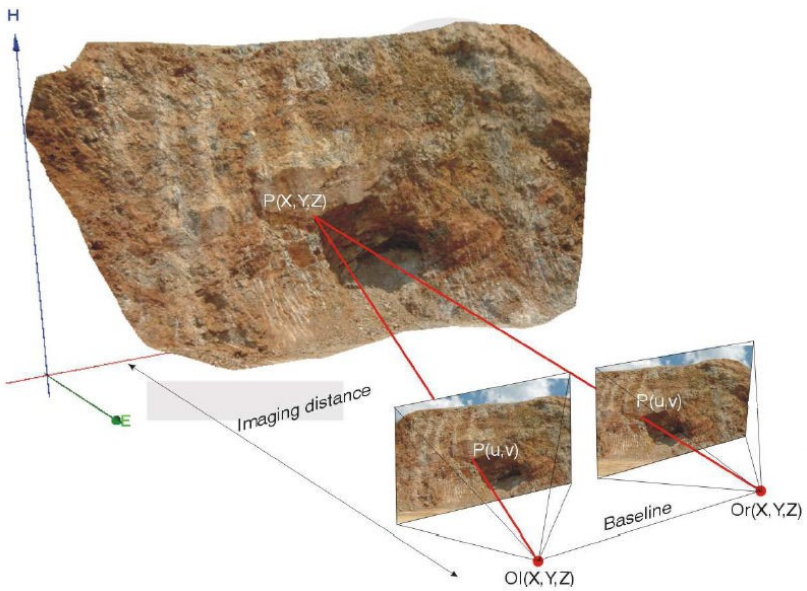

Figure 9: Creation of 3D point from two images taken from different positions at the site (ShapeMetriX^{3D} Manual, 2006, p. 2-3)

3.3 Scan Data

In this thesis three laser scan data sets are used:

- a quarry for testing the measurement methods of rock mass parameters
- a building (TU Graz) to compare the accuracies of different registration methods
- an underground excavation for introducing a new registration method

3.3.1 Angenofen

Near Stainz in southern Styria the U-shaped quarry of Angenofen is situated. It consists of grey to brown gneiss with cross joints that are nearly perpendicular to each other.

Due to the special orientation of the joints this quarry was chosen to test new methods for rock mass characterization with RiSCAN PRO.

3.3.1.1 Scan

The quarry was scanned in three scan positions at an average of 8 m distance to the wall. The scans were performed with different tilt angles and resolutions. Due to increasing cloudiness and subsequently limited GPS reception only from scan position 1, 2 and the remote object the GPS data was recorded. Altogether 15 tie objects (Chapter 3.4.2) were used (14 circles and 1 cylinder) and pinned to the wall. From the cylinder also the GPS data was recorded.

3.3.1.2 Data Post Processing

Since the GPS data of scan position 1 and the cylinder were available the registration was made via backsighting orientation (Chapter 3.5.1.2) to the global coordinate system.

Each wall of the U-shaped quarry was triangulated separately and then three models were combined. The final model was textured with the pictures collected during scan data acquisition. Figure 10 shows a photo-realistic model of the middle wall of the U-shaped quarry.

.

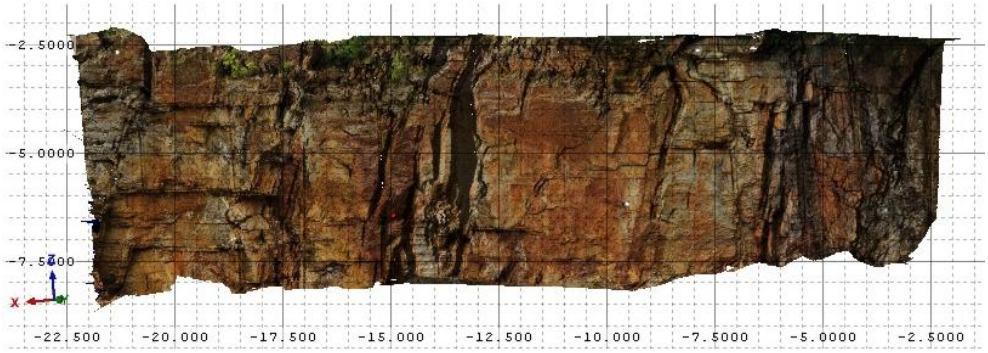

Figure 10: Final model, textured model of the middle wall of Angenofen

3.3.2 TU Graz

In November 2011 a scan survey was performed on a part of the building of TU Graz. The edges and windows of the building are convenient for testing the accuracy of different registration methods.
Three scan positions covered the scanned part of the building and 6 cylinders were installed. GPS data of all scan positions and of all but one cylinder was collected.
For application of different registration methods (Chapter 3.5.1) the deflection from north was measured at one scan position, an origin was defined and the direction from the origin to one scan position and to one cylinder was measured.

3.3.3 Arzberg

In December 2010 a LiDAR survey was performed in parts of a former lead-zinc mine near the village of Arzberg, north east of Graz.
Geologically Arzberg belongs to Graz Paleozoic, in detail to the “Arzbergschichten”. These consist of calcareous schist and black shale that carry lead and zinc mineralization (Faupl, 2003). Submarine hydrothermal activity formed metalliferous mud in which lead and zinc mineralization developed. The thickness of the mineralization varies from few centimeters to several meters (Weber, 2005).

3.3.3.1 Scan

Data was collected at a length of about 50 m between the “Nordschlag” and the “Arzbergschacht” part of the so-called “Raab”- gallery.
12 scan positions were completed using 5 cylinders as tie objects attached to racks of one meter. For data collection of the ridge the scanner had to be tilted several times to 90°.

3.3.3.2 Post Processing

As GPS data could not be collected a new registration method which was introduced by Liu and Kieffer (2012) was applied (Chapter 3.5.1.4). Additionally to the photos collected at each scan position also manual photos were taken.

Due to some dust in the air there were more ghost points than expected. These were eliminated partly by filtering the data with a 2.5 D – raster and partly by deleting the ghost points manually.

For creation of a model the 3D–triangulation method described in Chapter 3.5.2 was used. Figure 11 shows a small triangulated part of the gallery.

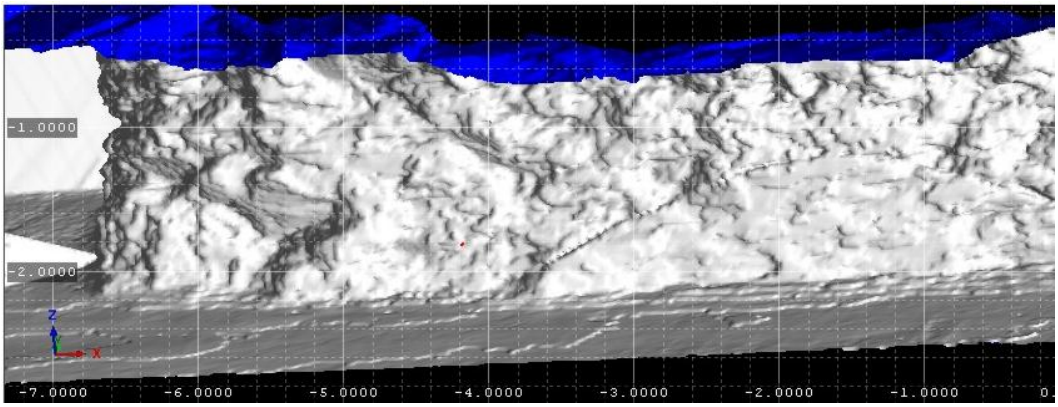

Figure 11: Model of a small part of the north wall of the gallery.

3.4 Field Data Acquisition

3.4.1 Definition of Scan Positions

“A scan position should be chosen to allow the maximum coverage of the study area, within the maximum range and angular field of view of the instrument (Buckley et al, 2008, p. 628).”

Since a scanned rock mass usually is not planar and the field of view of the scanner is limited, some surfaces might not be visible from only one

scan position. In these parts of the outcrop only few data ("shadow zone") or no data at all (occlusion) can be collected and they appear as black holes in the resulting point cloud (Chapter 3.4.5) (Kemeny et al, 2008). "Shadow zones" or zones of occlusion can occur horizontally as well as vertically (Figure 12) (Sturzenegger, 2009).

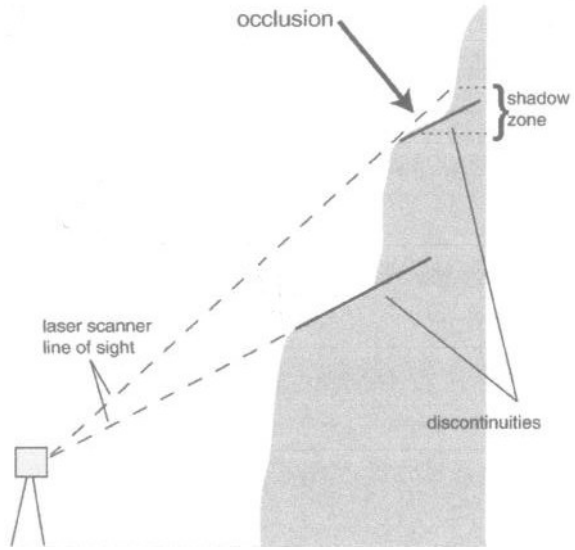

Figure 12: Occlusion occurs because the angle of the line of sight of the scanner is steeper than the discontinuity (modified after Sturzenegger, 2009).

To obtain data of the whole outcrop the scanner must be relocated several times to reduce or eliminate shadow zones. The different scan positions must overlap to minimize the shadow zones and to obtain the overall picture of the scanned outcrop (Figure 13). Buckley (2008) states that the overlap of the scans should increase with rising complexity of the outcrop.

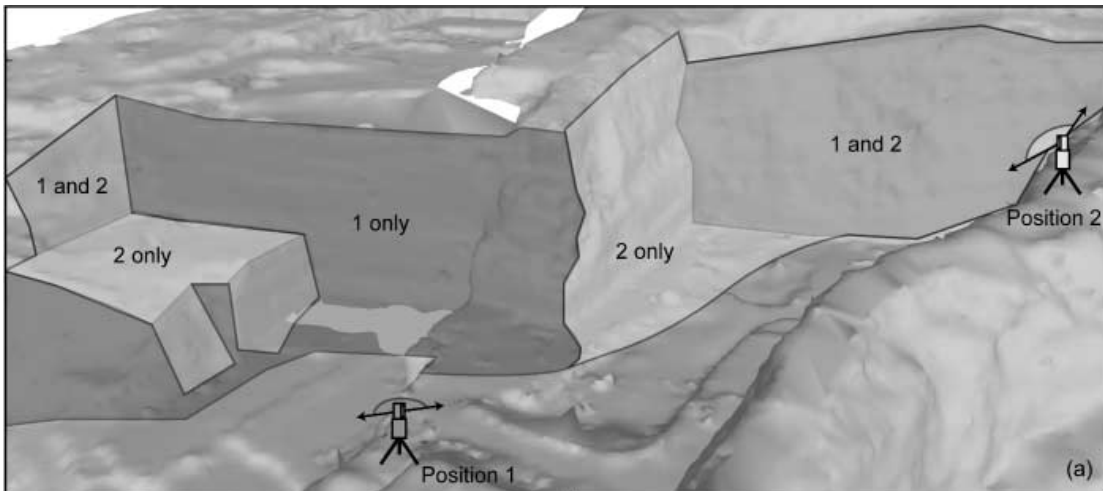

Figure 13: To collect data of the whole outcrop two overlapping scan positions are necessary. (Buckley, 2008, p. 628).

By tilting the scanner more data is obtained vertically (Figure 14) but to gain the best results the scanner should be positioned orthogonally to the scanned outcrop without tilting. If the outcrop has a large vertical extension “an elevated scan position, typically from the opposite side of the canyon or valley (Buckley et al, 2008, p. 629)” reduces vertical shadow zones (Buckley et al, 2008).

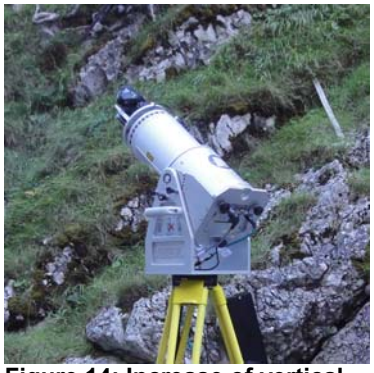

Figure 14: Increase of vertical data acquisition by tilting the scanner (Macher, 2010).

Another aspect which should be considered when defining different scan positions is vegetation and other objects that might cause shadow zones. If possible scan positions should be chosen on locations where vegetation or other objects do not interfere the line of sight of the scanner (Buckley et al, 2008).

3.4.2 Installation of Reflector Targets

For registration of scan data (Chapter 3.5.1) control points (tie points) need to be installed. For this purpose circular or cylindrical retroreflectors are used (Figure 15) (Link 6) that reflect the laser beam with a minimum of scattering of the light.

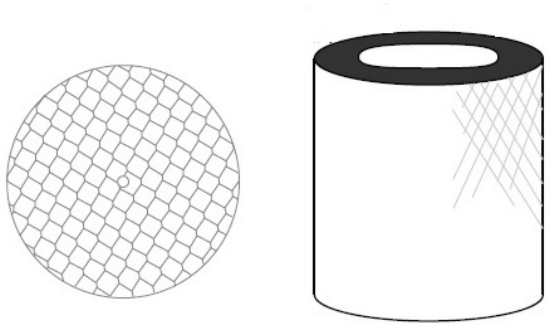

Figure 15: Circular or cylindrical retroreflectors can be used as tie points (modified after Link 6)

Circular tie points can be pinned directly onto the rock whereas cylindrical control points must be placed on horizontal discontinuity surfaces or on brackets. For registration of the various scan positions at least three tie points must be visible from each scan position (Riegl, 2006).

Sometimes the mounting of tie points is not possible if the installation of targets is too dangerous or if the distance between the scanned outcrop and position of the scan survey is too large. Then registration can be accomplished without reflectors, though it will take more time (Chapter 3.5.1.3).

3.4.3 Scan Data Acquisition

Before data acquisition an overview-scan with low resolution should be performed using the total field of view of the scanner. This gives the surveyor an idea where the outcrop is located in the field of view of the scanner. For a detailed acquisition of the outcrop a scan with defined

horizontal and vertical scanning range and angle resolution (horizontal and vertical) must be defined. The range should cover the area of interest. The resolution, defined in degrees, determines the interval of the laser shots and consequently the point density. If for example the resolution is 0.2 (vertical and horizontal) laser shots are separated by 0.2 degrees both horizontally and vertically.

The highest angular resolution that can be achieved for scan data is 0.02 (Riegl LMS Z 620). The actual point density depends on the distance between the scanner and the outcrop. The relation between the resolution (φ), the distance to the outcrop (R) and the point spacing (d) is shown in Figure 16a).

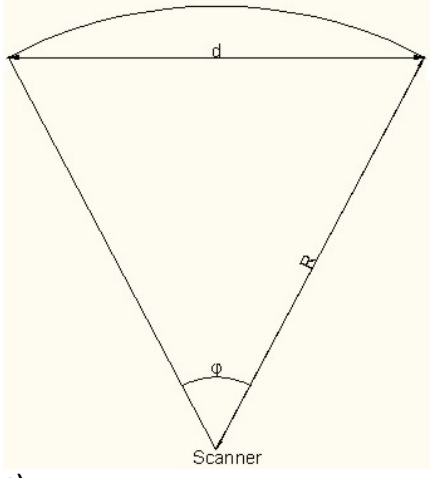

a)

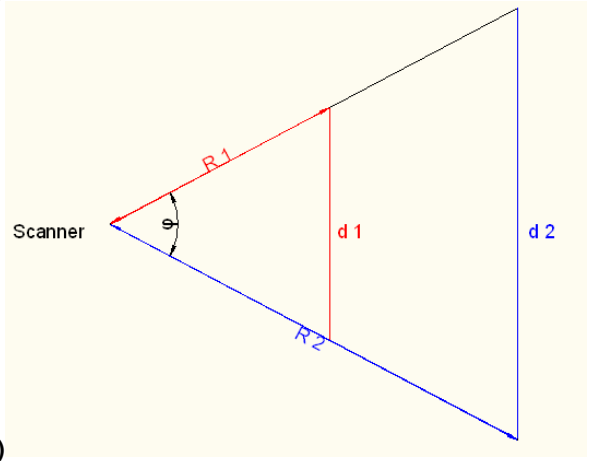

b)

Figure 16

The larger the distance to the outcrop, the larger the spacing between two points and consequently the lower the point density (Figure 16b). Equation 8 results out of Figure 16a):

$$d = 2R \cdot \sin\frac{\varphi}{2}$$

Equation 8

Example: A scan which was performed with a resolution of 0.07° at a distance of 10 m to the outcrop has a point spacing of 1.2 cm. If a scan with the same scan resolution was performed at a distance of 100 m the point spacing is 12 cm.

In general the resolution should be adapted to the purpose of the scan and the available time (Buckley et al, 2008), "e.g. centimetre point spacing is probably not required when capturing the 3D geometry of a series of beds in a cliff section of a kilometre extent (Buckley et al, 2008, p.627)."

Figure 17: The camera (red circle) and the GPS receiver (blue circle) fixed on the scanner.

3.4.4 Image and RTK-GPS Data Acquisition

Photos from each scan position are automatically taken with a camera mounted on the scanner (Figure 17). They are used for coloring the scan data or a model to produce a photo-realistic reproduction of the scanned area (Chapter 3.5.3).

For accurate determination of a scan

position a RTK-GPS receiver is mounted on the scanner (Figure 17). With the receiver fixed on a bracket GPS-coordinates can be collected from reflector targets (tie points) as well. The acquisition of GPS-coordinates can be used for an accurate registration (Chapter 3.5.1.1).

3.4.5 Point Cloud

The result of each scan is a three-dimensional point cloud (Figure 18). Since the scanner does not make a distinction between rock mass and other objects like vegetation, cars or people, the original point cloud contains lots of points that do not belong to the object of interest. These points are so called “ghost points” and must be deleted before modeling by applying different filter operations.

Figure 18: A point cloud of a part of the quarry in Angenofen.

3.5 Data Post Processing

3.5.1 Registration

As mentioned in Chapter 2.1 the scanner has its own coordinate system (SOCS). Therefore data acquisition from different scan positions indicates different x-, y- and z-coordinates for one point. For further processing of the point clouds these coordinates have to be merged to one superior coordinate system by translating and rotating the point clouds. This process is called “registration”. The superior coordinate system can either be a so-called “Project Coordinate System” (PRCS) or the Global Coordinate System (GLCS), if GPS data was collected (RiSCAN PRO Manual) (Figure 19). If it is possible to register the point clouds into the GLCS, the x-, y- and z-axis are equal to east, north and the elevation.

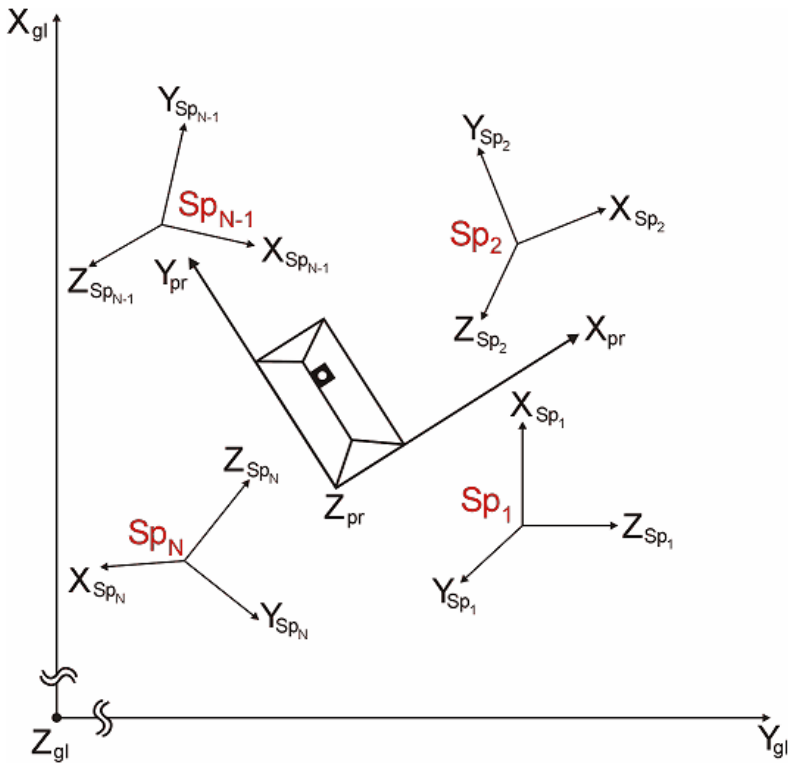

Figure 19: Hierachy of different coordinate systems (Manual of RiSCAN PRO, p.36)

Figure 20a) shows two point clouds of two different scan positions that are not yet registered. The cupola of the roof was marked with a red point both in the photo (Figure 20b) as well as in the point clouds (P_1 and P_2). Since the point clouds belong to two different scan positions, P_1 and P_2 have different coordinates, although the points were created on the same spot of the cupola.

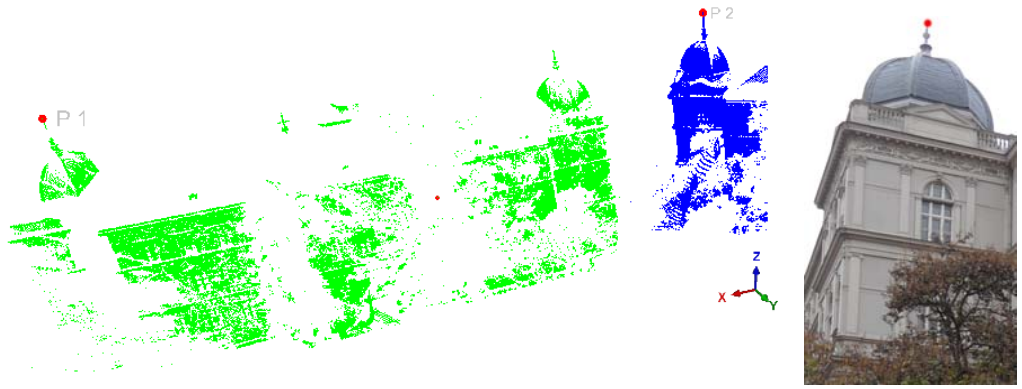

Figure 20 a) **b)**

Based on the Manual of RiSCAN PRO following methods are described:

- Registration via GPS-coordinates
- Backsighting with known global coordinates
- Coarse Registration and Multi Station Adjustment
- Backsighting without known global coordinates

3.5.1.1 Registration via GPS-Coordinates

For this registration method coordinates of each scan position as well as of tie points have to be collected by using a RTK-GPS. After data acquisition the RTK-GPS data can be used for a highly accurate registration assuming that no sources of interface were affecting the GPS-reception.

For registration in RiSCAN PRO the coordinates are then simply copied into the tie point list of the GLCS. Before registration of the scan positions a transformation of these coordinates has to be performed because the PRCS works only with numbers smaller than 9999. Then the scan positions can be registered by common tie points. As an example the result of registration via GPS-coordinates is shown in Figure 21.

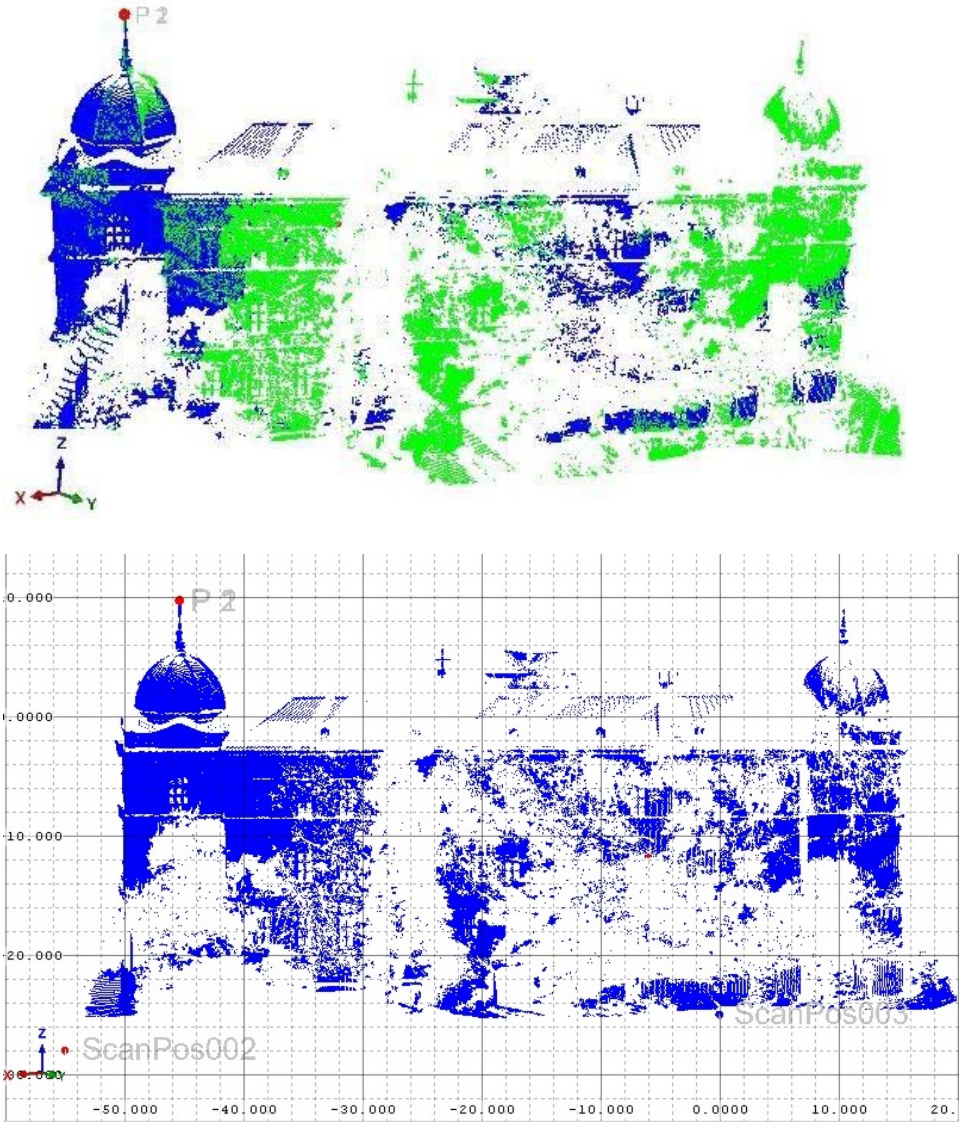

Figure 21: Registered with all GPS-coordinates known.

3.5.1.2 Backsighting with Known Global Coordinates

Registration via backsighting means that the coordinates from one scan position (Figure 22) and either a remote object (Figure 23) or the deflection from north (northing angle) (Figure 24 a & b) are known.

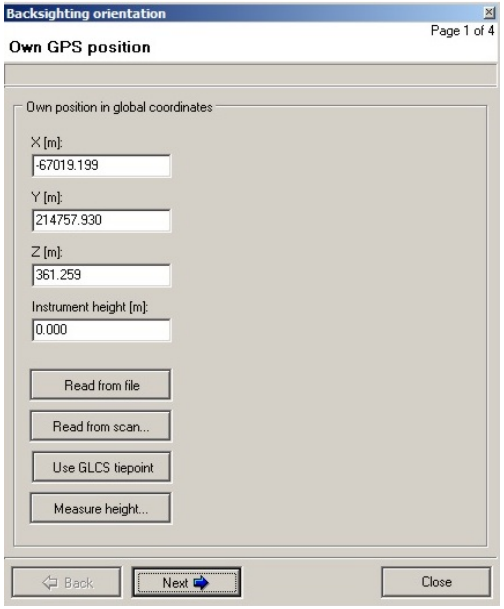

Figure 22: Window for entering the coordinates of the scan position.

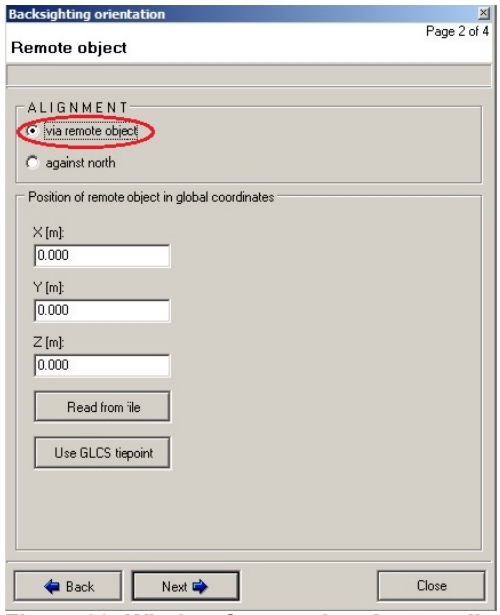

Figure 23: Window for entering the coordinates of the remote object.

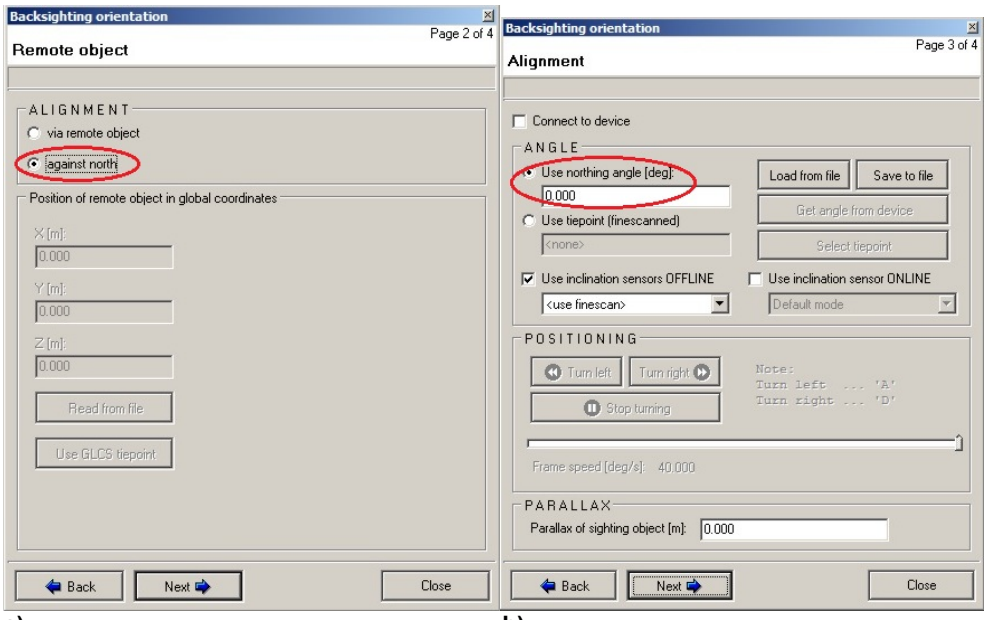

a) **b)**

Figure 24: Backsighting against north (a) requires the entry of the deflection from north (b)

When using backsighting via a remote object either a fixed object with known coordinates (buildings whose position is known or can be determined by GPS) or reflectors installed for the scan (tie points) must be chosen. In this thesis tie points are used. It is important to know the height of the remote object as well as of the laser scanner. The height of the laser scanner is defined as “the vertical offset between the well known ground point and the laser beam exit (Manual of RiSCAN PRO, p.181)”.

When registered the y-axis is equal to north. For using “backsighting orientation” the deflection (β) of the scanner’s y-axis (y-axis of SOCS) from north has to be measured (Figure 25).

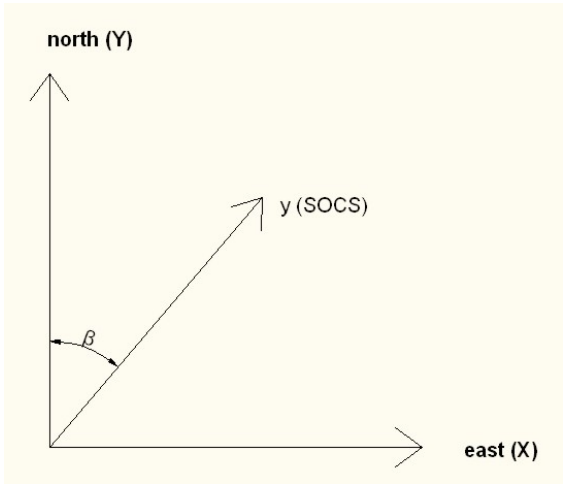

Figure 25

Further scan positions can then be registered based on common tie points (Figure 26).

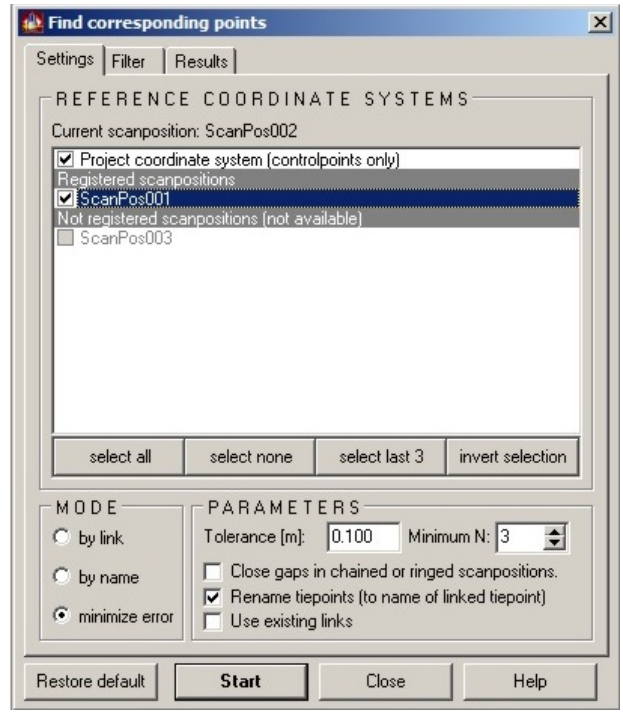

Figure 26: Registration via common tie points for the remaining scan positions

In RiSCAN PRO at least three common tie points have to match the various scan positions. The more tie points that correspond to the different scan positions, the more accurate the registration.
Figure 27 shows the two point clouds (P_2 covers P_1) of Figure 20a) registered by backsighting orientation.

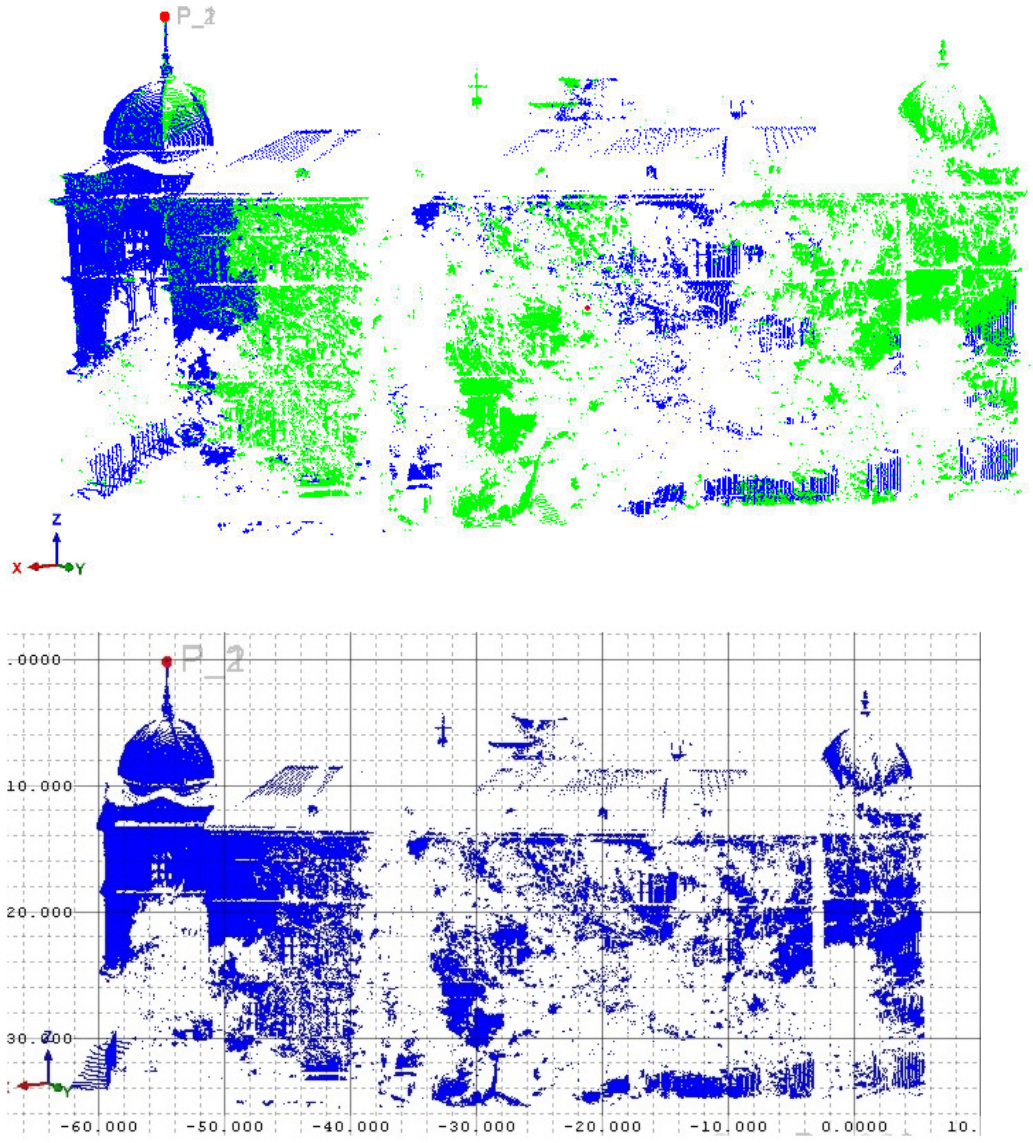

Figure 27: Registered via Backsighting with known global coordinates.

3.5.1.3 Coarse Registration and Multi Station Adjustment

This method is used if one scan position has already been registered (e.g. by backsighting against north) but no reflectors (tie points) are available. In this case the registration can be done manually using this registered scan position as reference. Points are created on the same spots of distinctive features (e.g. roofs, cars) in the reference scan position as well as in the point cloud, which is not registered. For effective registration at least four point pairs should be chosen. The registration is performed by using the created points as “tie points”.
Using manual coarse registration is less accurate compared to other registration methods because usually not exactly the same points are marked in both point clouds. To increase the accuracy of the registration a so-called Multi Station Adjustment (MSA) should be applied. “The MSA tries to improve the registration of the scan positions. For that purpose the orientation and position of each scan position is modified in several iterations in order to calculate the best overall fit for them. To compare the scan positions the [..] polydata objects (reduced point clouds) are used. (Manual of RiSCAN PRO, p. 192)”
Figure 28 shows again the two point clouds from Chapter 3.5.1, now registered with coarse registration and MSA (P_2 covers P_1).

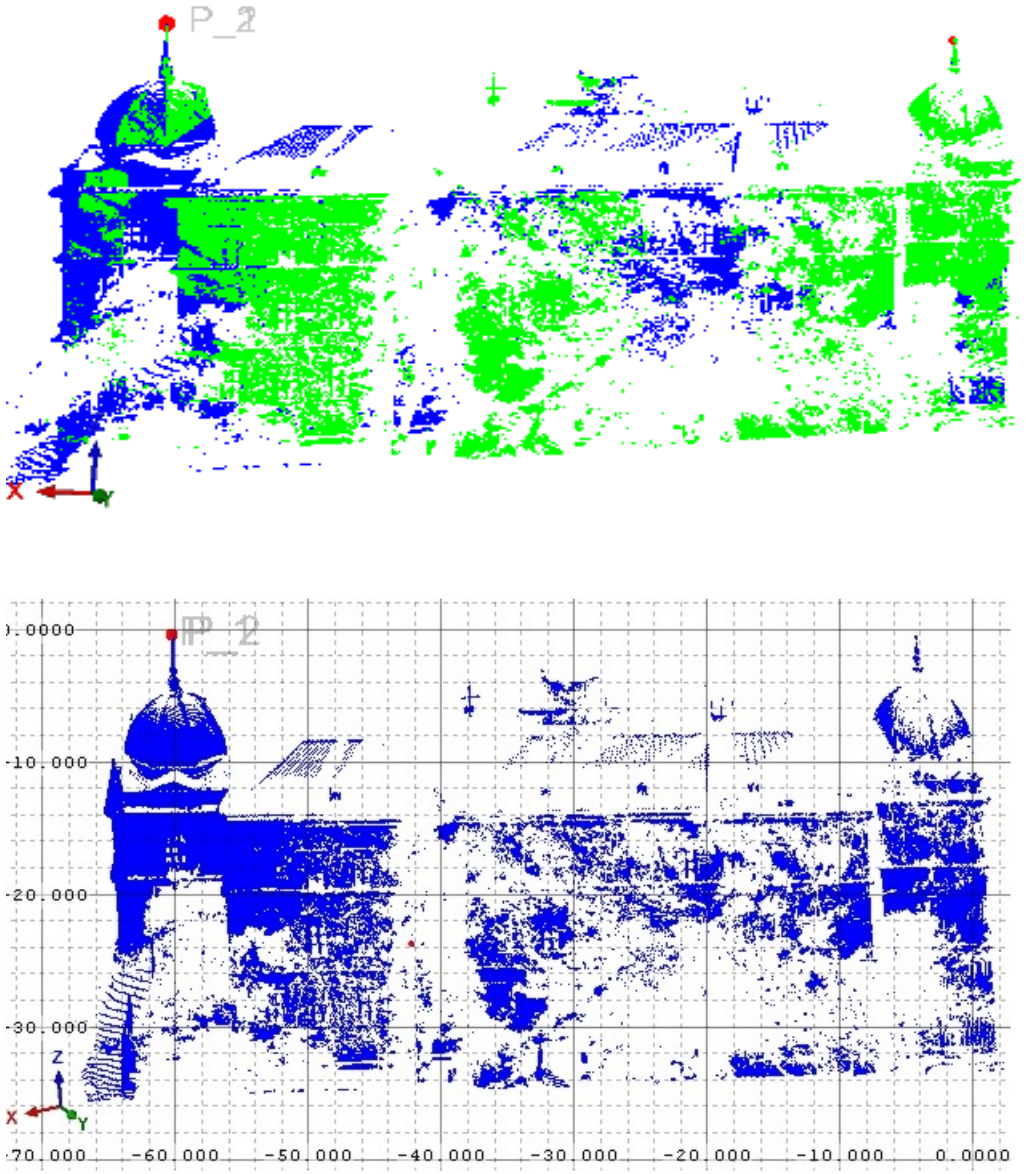

Figure 28: Registered with coarse Registration and MSA

3.5.1.4 Backsighting without Global Coordinates

In some cases, especially in tunnels, it is impossible to work with a GPS. Nevertheless in geology the collection of orientations of discontinuities is important. Therefore another registration method was developed (Liu and Kieffer, 2012) in addition to the methods described in the Manual of RiSCAN PRO. This method defines an origin in the area of interest.

Then the distance from the origin to the first scan position and a remote object is measured and the deflection of the geographic north is determined. As both heights (scanner and remote object) are known, the coordinates of the scanner and the remote object can be calculated with Equations 10 and 11, assuming that the y- axis reflects north.

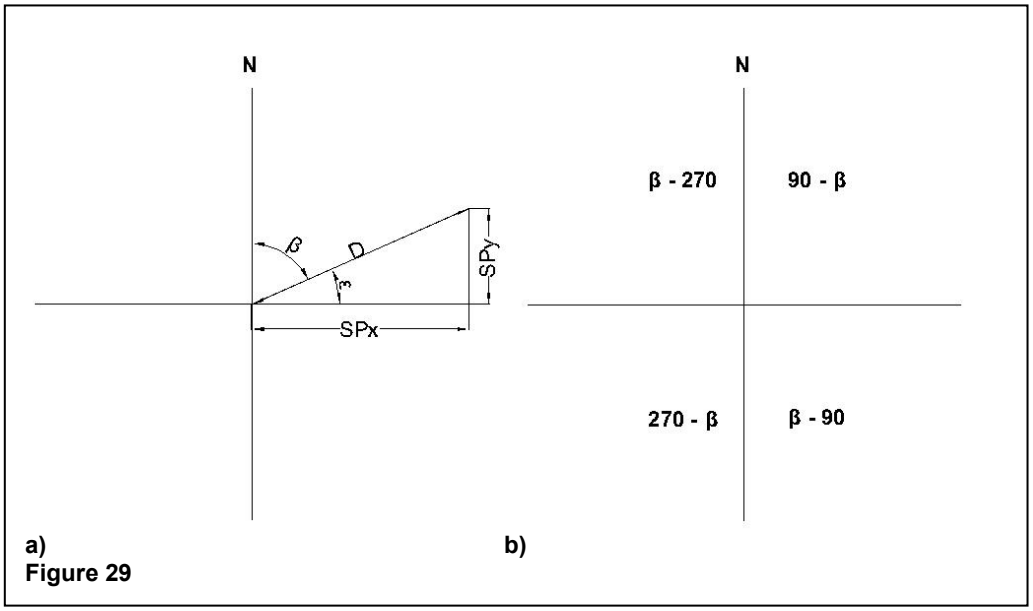

a) b)

Figure 29

Let β be the deflection from north, D the measured distance between the origin and the scan position and SPx /SPy the unknown coordinates of the scan position. The following Equations are based on Figure 29a):

$$\varepsilon = 90 - \beta$$ **Equation 9**

$$SPx = D \cdot \cos \varepsilon$$ **Equation 10**

$$Spy = D \cdot \sin \varepsilon$$ **Equation 11**

Depending on the quadrant in which the scan position is located β must either be subtracted from 270° or 90° or these two values have to be deducted from the deflection (Figure 29b) (Equation 9). The different

algebraic signs of x- and y- coordinates for each quadrant must be considered.

Using the β value for the remote object, its coordinates can be calculated with the Equations 10 and 11 as well.

In a last step the other scan positions can be deducted with the backsighting function in RiSCAN PRO.

Though global coordinates cannot be read with this method, orientations of discontinuities can be measured. The result of registration with this method is shown in Figure 30.

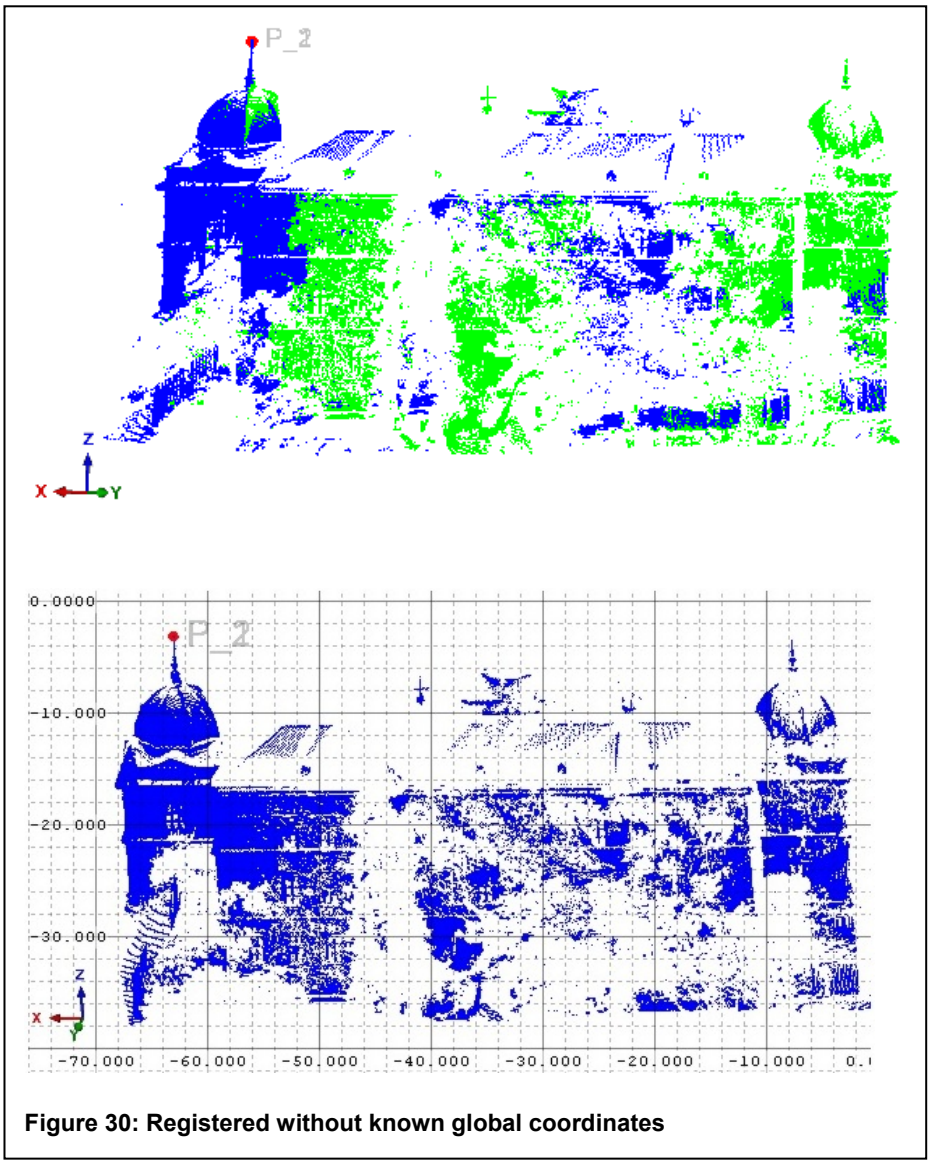

Figure 30: Registered without known global coordinates

Figure 31a-d) shows a comparison of the four different registration methods used on the basis of a detailed view of the cupola. The accuracy of different registration methods will be discussed in Chapter 4.1.

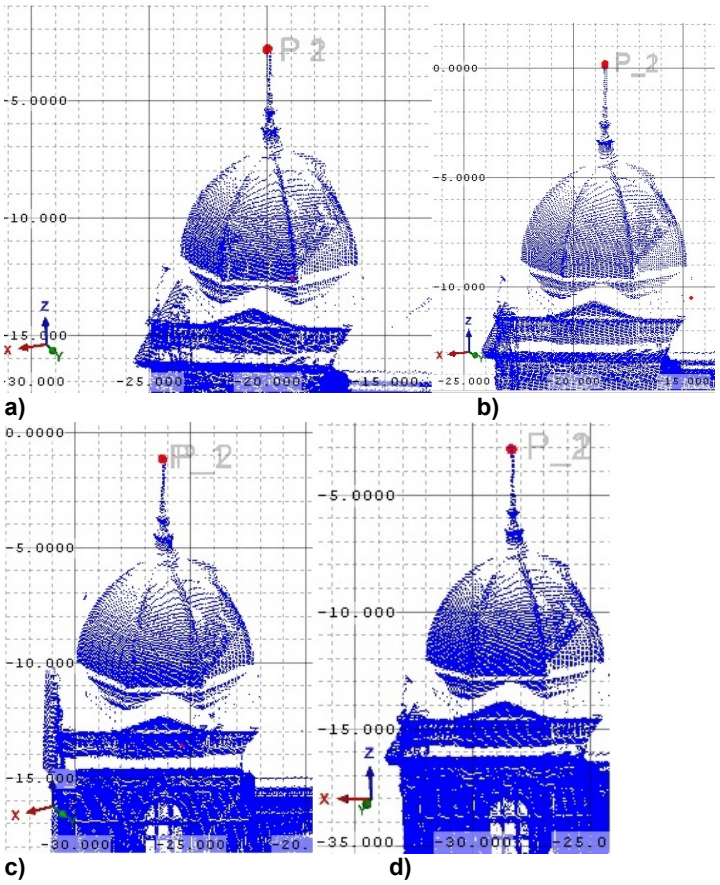

Figure 31: Registration with known GPS coordinates (a), backsighting with known global coordinates (b), coarse registration and MSA (c), backsighting without known global coordinates (d)

3.5.2 Triangulation

Triangulation still has to be performed, although the main structures of a rock mass are visible in a point cloud.

Basically a triangulation is the generation of a closed surface by connecting adjacent points to triangles. RiSCAN PRO uses the so-called "Delauny Triangulation" which follows the circumcircle principle. That

means that the circumcircle of one triangle must not contain any other points. The result of this process is called mesh or TIN (triangulated irregular network) and is a morphologically realistic model of the scanned area. To get the best result only cleaned data should be used.
The difference between a point cloud and a mesh is shown in Figure 32.

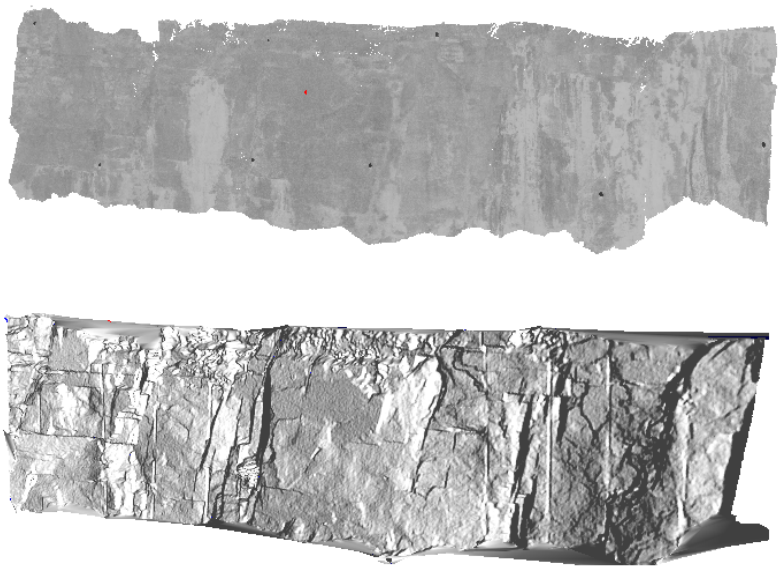

Figure 32: Difference between a point cloud (above) and a surface mesh (below)

RiSCAN PRO offers three main triangulation modes, i.e. polar triangulation (3D-triangulation), volume triangulation and plane triangulation. The latter projects the points to a plane and depends on the viewport (Manual of RiSCAN PRO). So the point cloud has to be rotated and only the points of the current sight can be processed properly. However, during work with this method it turned out that the poor resolution might influence parameters for rock mass characterization like roughness. Figure 33 a) & b) shows the difference between resolutions of plane triangulation and volume triangulation which is described below and was used for modeling of walls and quarries in this thesis.

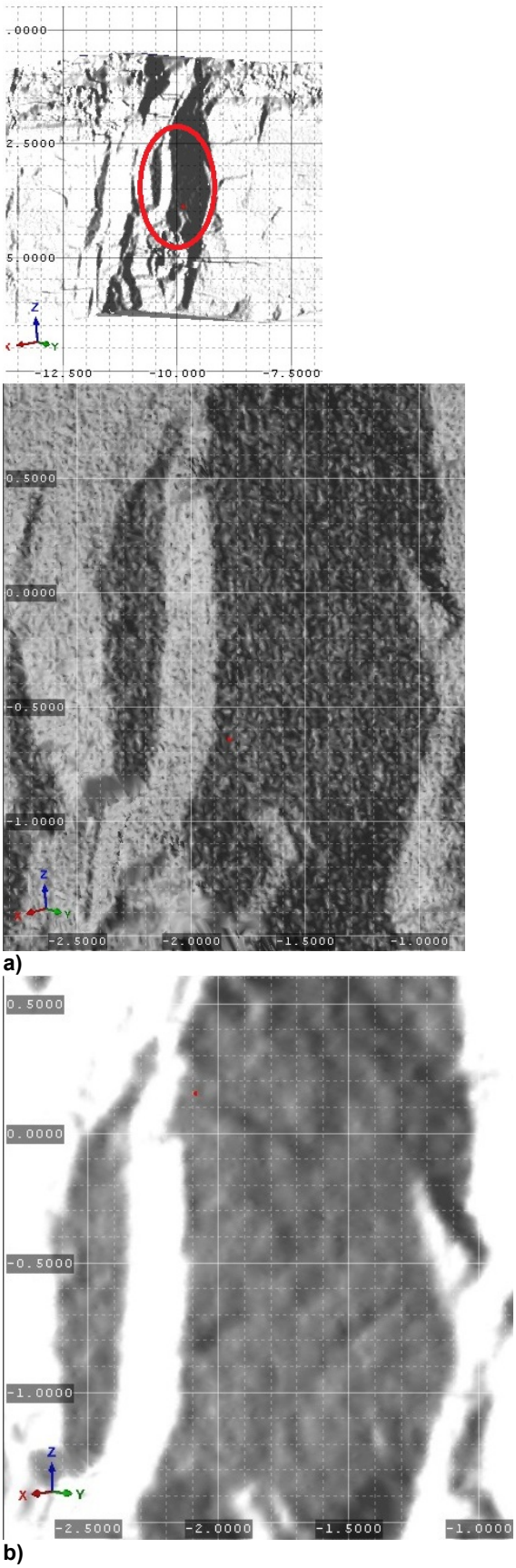

Figure 33: Plane triangulation with poor resolution (a) and volume triangulation (b)

Volume triangulation is similar to plane triangulation but a raster is put to the reference plane which is parallel to the model. The size of the raster defines the pattern that is filled with the data (Manual of RiSCAN PRO). Then a 2D-Delauny triangulation is performed "from the 2D coordinates of the vertices mapped onto the reference plane (Manual of RiSCAN PRO, p.268)".

Triangles, created between the reference plane and the model, might cover geological structures from certain viewports and should be deleted (Figure 34 a & b).

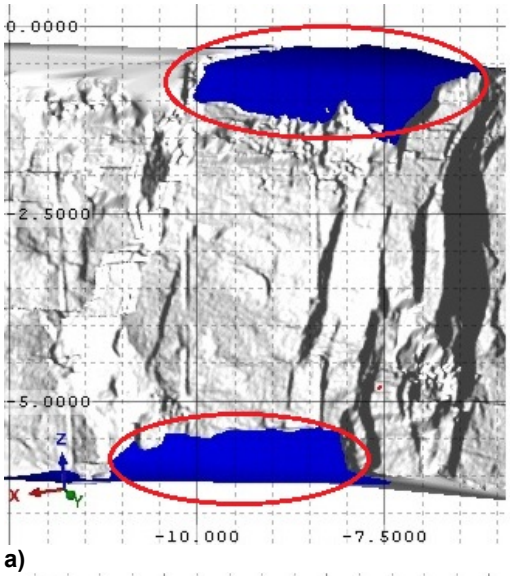

a)

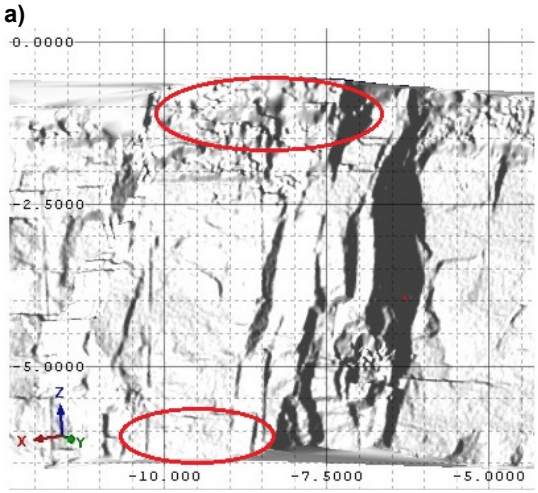

b)

Figure 34: Triangles that cover part of the surface of the rock mass (a) should be deleted (b)

The polar triangulation is independent of the viewport. “In order to perform a polar projection of the data points the function needs to know the position from where the data was recorded (scan position) (Manual of RiSCAN PRO, p.220)”. With the function “extract outer surface” this triangulation method is useful when processing tunnels.

3.5.3 Texturing

The mesh resulting of triangulation is always monochrome. To get a photo-realistic model of the scanned area the mesh can be colored with the pictures taken by the camera mounted on the scanner. This procedure is called texturing. However, “images […] might be slightly distorted by the lens (Manual of RiSCAN PRO, p.233)”. Therefore it is important that all images used for coloring the model are undistorted.
During progression of the thesis it showed that although a colored model is useful for presentation purposes and also for defining stages of weathering, it is more advisable to use the monochrome mesh for further measurements because it is easier to distinguish objects like planes or polylines from the surface mesh.

3.6 Discontinuity Characterization with RiSCAN PRO

RiSCAN PRO offers some geometric functions that may be used for measurement and calculation of parameters explained in Chapter 2.2.
This might be a big advantage if structures in a rock mass that seem important are not accessible for hand measurement.
This chapter describes the methodology of determining discontinuity parameters with RiSCAN PRO.

3.6.1 Scanline

In RiSCAN PRO the front edge of a plane which intersects the model is defined as a scanline. Data of all discontinuities that intersect this plane

is collected. Since for measurements like apparent spacing the intersection points have to be along a line, planes are created out of the discontinuity surfaces and intersected with the front edge (Figure 35 a & b) of the plane which was defined as the scanline.

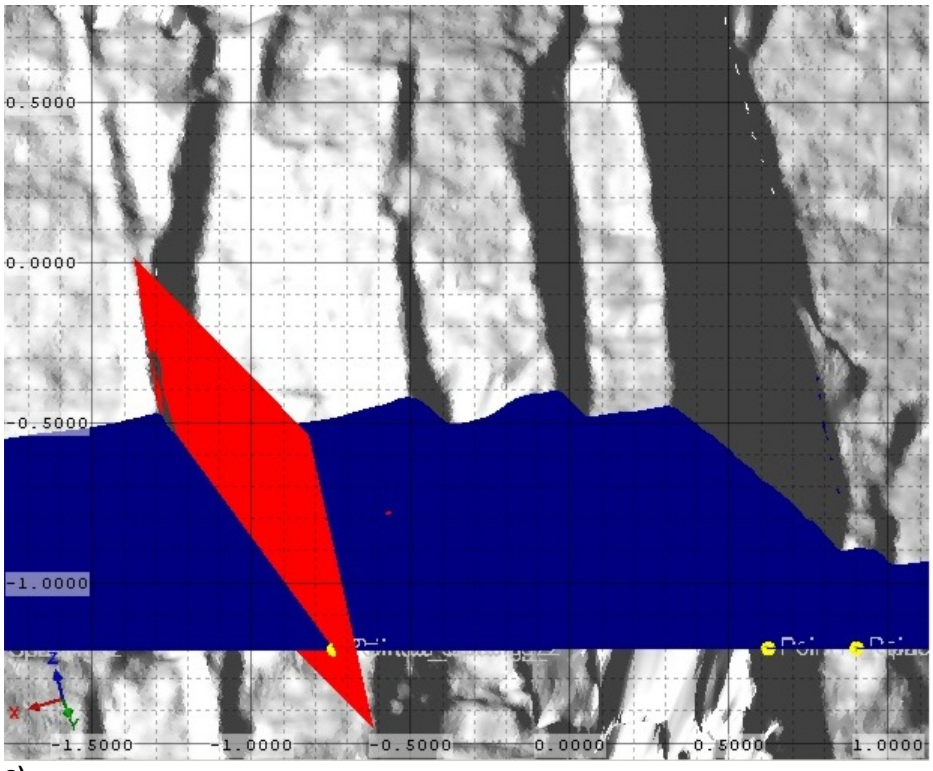

a)

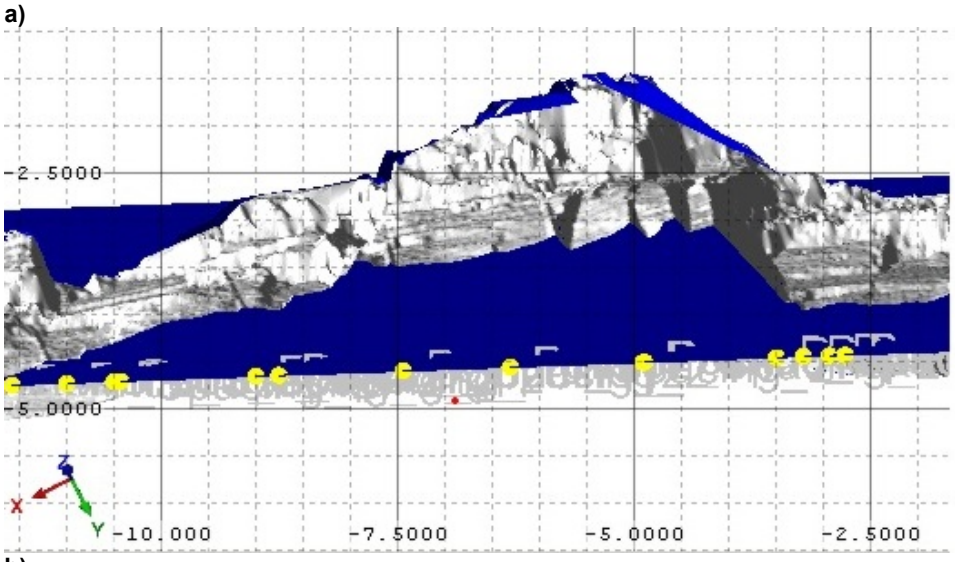

b)

Figure 35: A plane created out of a discontinuity surface intersects the front edge of the scanline (blue) (a). Intersection points (yellow) of different discontinuity surfaces (b).

3.6.2 Determination of Orientation

In this thesis two methods of orientation determination and analysis are described.

Both methods assume that the data set was registered before, at least to the north angle, so that the true north direction is given by the y-axis.

3.6.2.1 Measuring Orientation with RiSCAN PRO

In a first step a representative part of a discontinuity surface has to be selected in the dataset. Then a plane is created out of this selection with the function offered by RiSCAN PRO “create plane from selected area” (Figure 36a). In the plane’s info box (Figure 36b) the dip angle and dip direction are already given and can be copied to an excel file for further use. This is then continued with all further planes of interest.

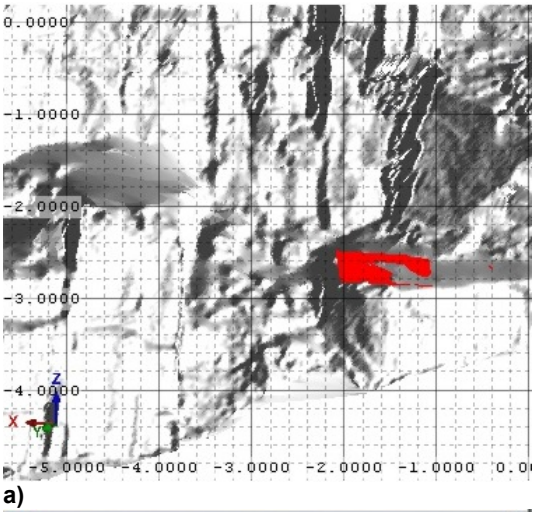

a)

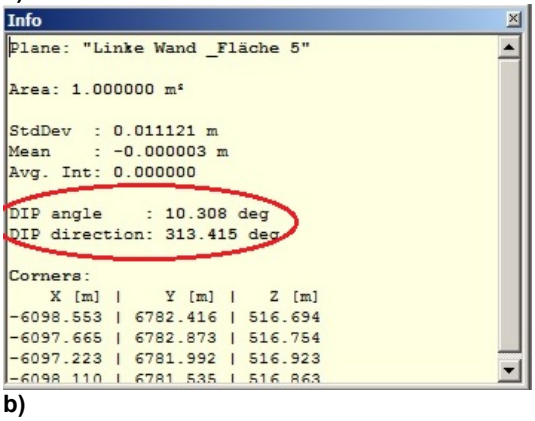

b)

Figure 36: A plane crated out of a discontinuity surface (a) and its orientation (b).

3.6.2.2 Determination of Orientation with Direction Cosines

If the processing software does not determine dip direction and dip angle automatically, these parameters can be calculated by creating a plane out of the discontinuity surface and using the normal's coordinates of this plane for calculation of dip angle and dip direction.

The equations below result from Figure 37.

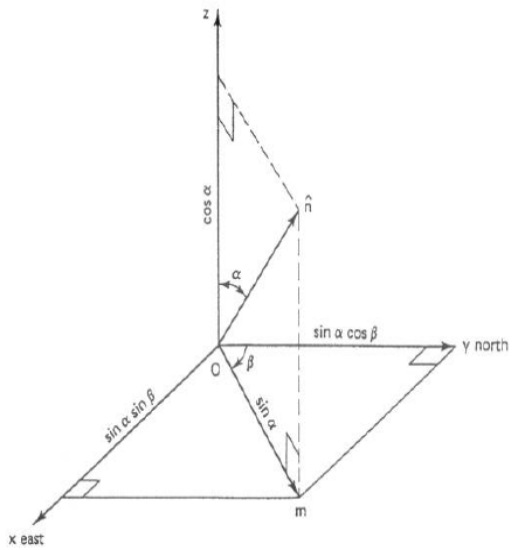

Figure 37: "Coordinate system and direction cosines of a normal" (Goodman, 1985, p. 27).

$$x = \sin\alpha \cdot sin\beta$$ **Equation 12**

$$y = \sin\alpha \cdot \cos\beta$$ **Equation 13**

$$z = \cos\alpha$$ **Equation 14**

(Goodman, 1985)

By converting above equation the dip angle and dip direction can be determined:

$$\alpha = \arccos z$$ **Equation 15**

$$\beta = \arccos\left(\frac{y}{\sin\alpha}\right)$$ **Equation 16**

3.6.3 Spacing

With RiSCAN PRO both apparent as well as true spacing can be determined. For measuring the apparent spacing a plane with the same spatial orientation as a discontinuity surface is extended till it intersects with the scanline. The intersection is marked by a point. With the command “measure distance” the linear distance between two points of intersection is determined (Figure 38 a & b).

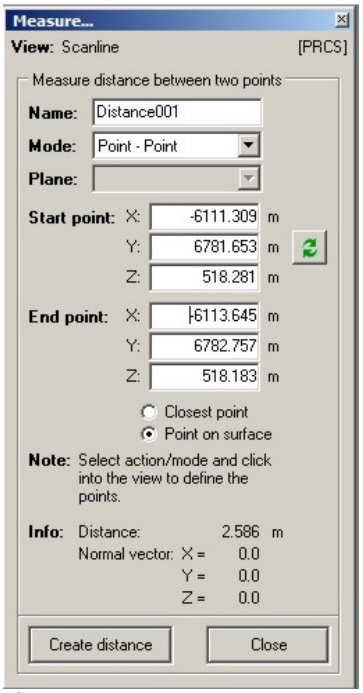

a)

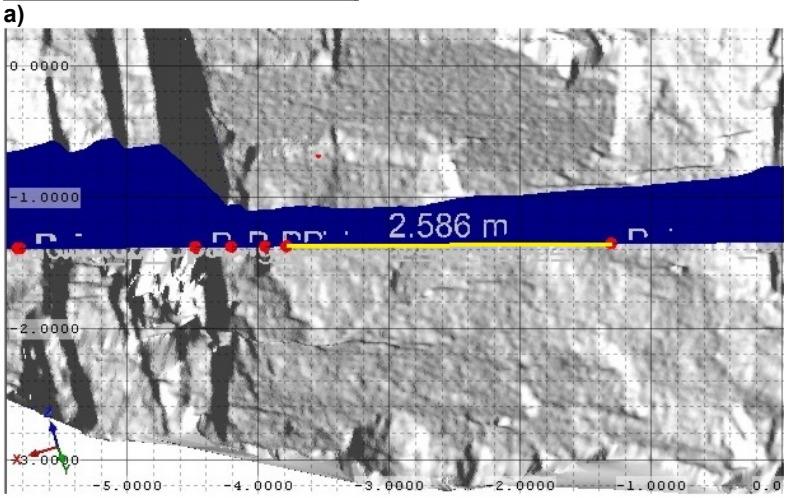

b)

Figure 38: With the command "measure distance" (a) the linear distance between two points is determined (b)

Calculation of the true spacing requires more effort. First of all the orientation centroid of each joint set must be calculated. By using these values the coordinates for the corresponding plane normal can be determined based on Equations 12 to 14 from Chapter 3.6.2.2. In a next step any plane can be created in RiSCAN PRO. The calculated values for the plane normal are inserted in the plane properties (Figure 39a). This changes the orientation to match the orientation of the centroid-plane of the particular joint set (Figure 39b).

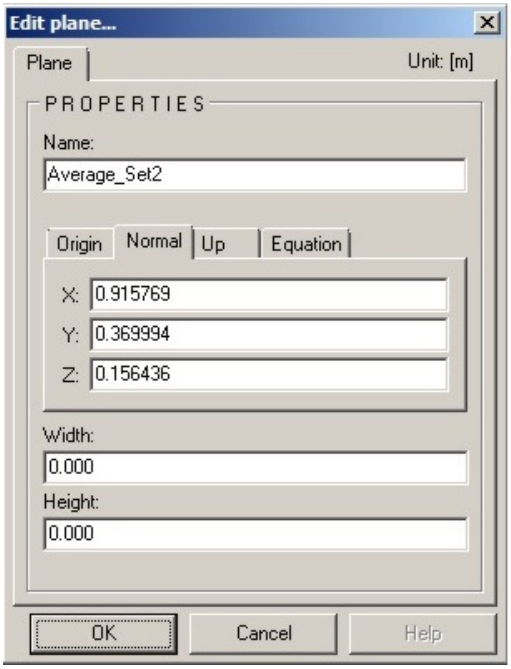

a)

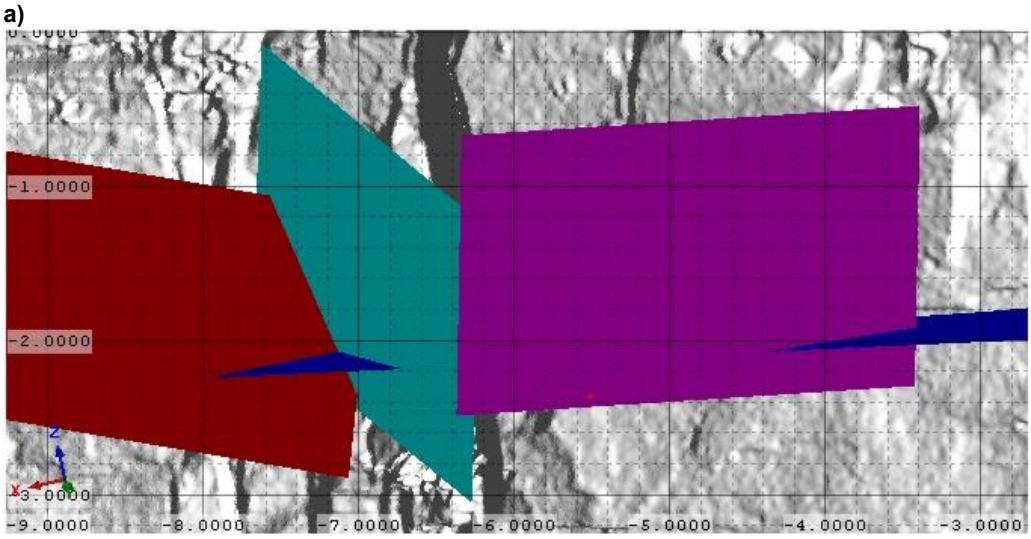

b)

Figure 39: a) shows the window where the plane coordinates can be entered and b) shows average planes of three joint sets, that intersect with the scanline (blue).

To achieve maximum accuracy the coordinates of the normal must be calculated with at least 3 decimal places otherwise the program generates planes with best fitting coordinates.

Next the angle ε between the centroid-plane and the scanline is measured with the command “calculate angle” (Figure 40 a & b).

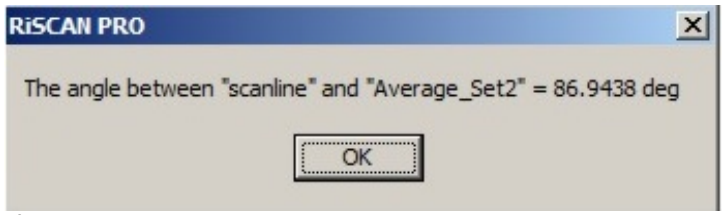

a)

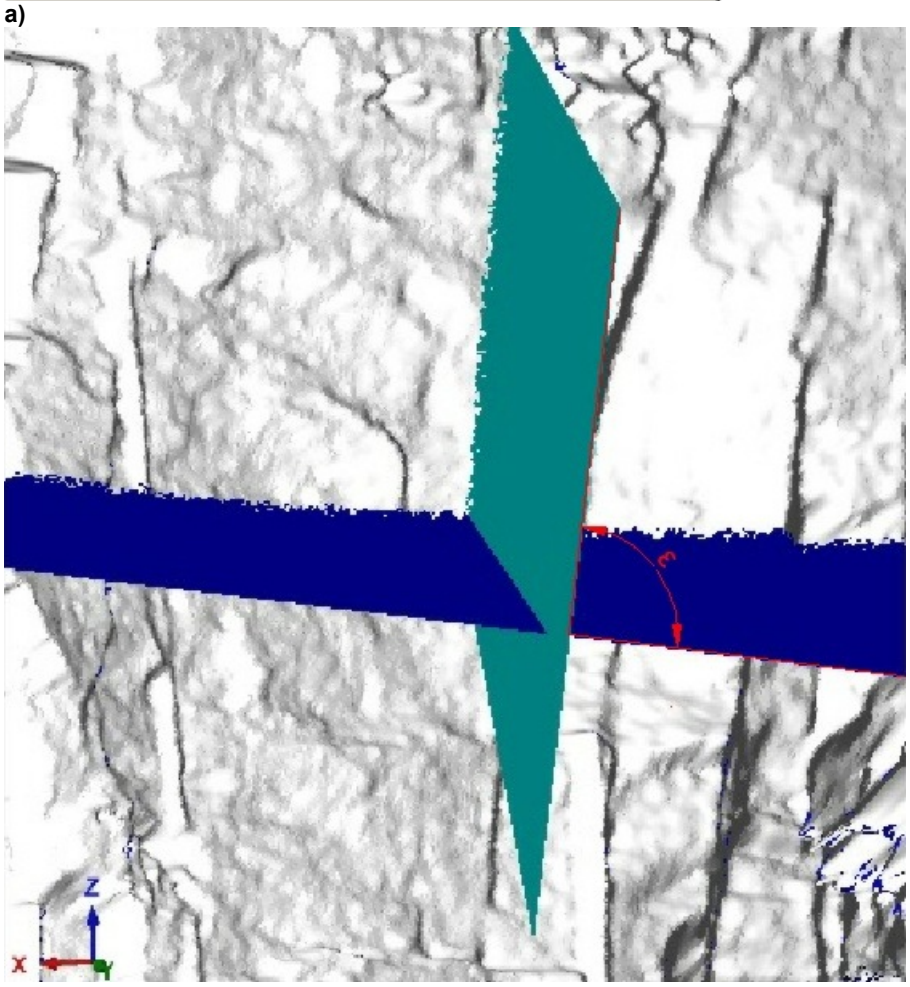

b)

Figure 40: The measured angle ε (a) between a plane and the scanline (b)

Figure 41 shows the geometric relation between ε, the measured apparent spacing (AP) and the true spacing (R).

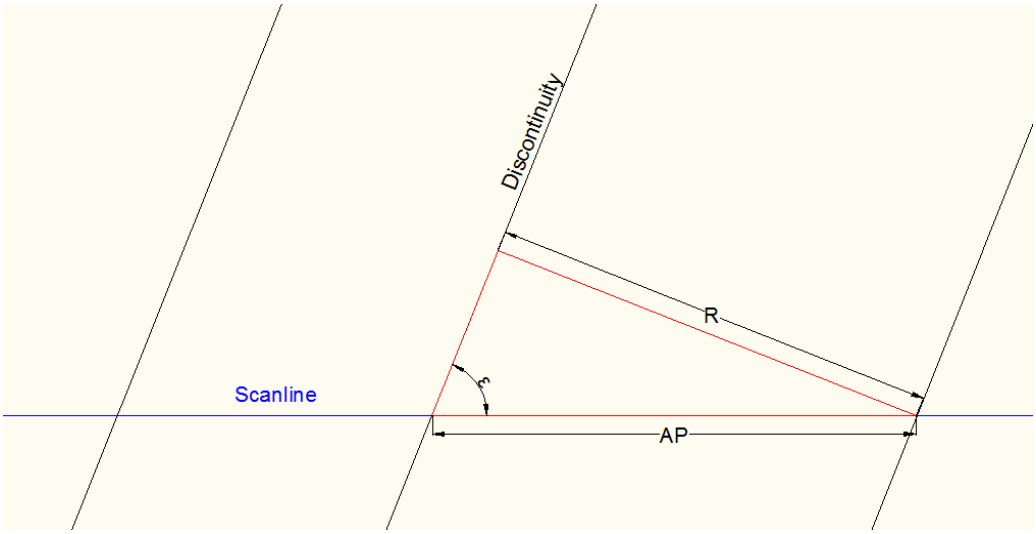

Figure 41: Relation between ε, apparent spacing (AP) and true spacing (R).

For calculation of the true spacing (R) Equation 17 which results out of Figure 41 is used:

$$R = AP \cdot \sin \varepsilon$$

Equation 17

In addition linear frequency can be determined as mentioned in Chapter 2.2.4.

3.6.4 Trace Length

Trace lengths are determined by selecting a discontinuity surface including its trace (Figure 42a) and creating a limited plane (command: "Create limited plane from selected area" (Figure 42b). The length of the plane is the interpreted trace length of the discontinuity and is given in the plane properties (Figure 42c).

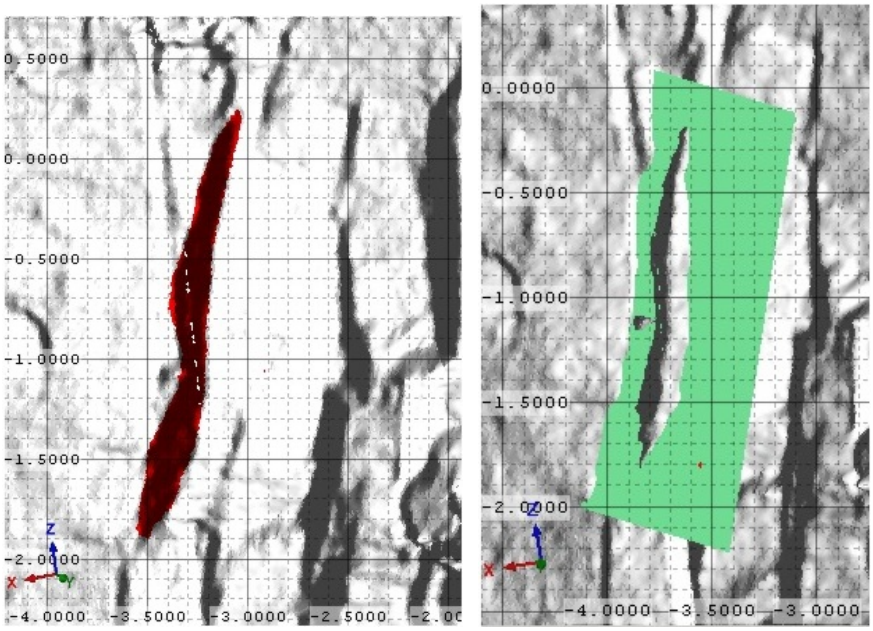

a)

b)

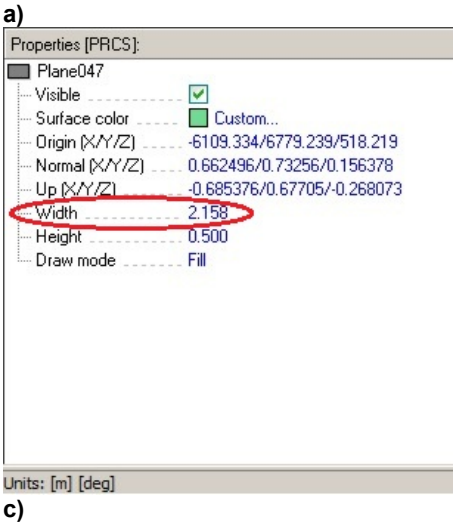

c)

Figure 42

Simultaneously terminations for each trace can be recorded.

3.6.5 Roughness

Roughness can be determined by comparison of profiles after Barton (ISRM, 1981) as well as by calculation of undulation after Palmström (2001) (Chapter 2.2.7).

3.6.5.1 Estimation of Roughness after Barton

In a first step a discontinuity surface which intersects with the scanline must be selected (Figure 43).

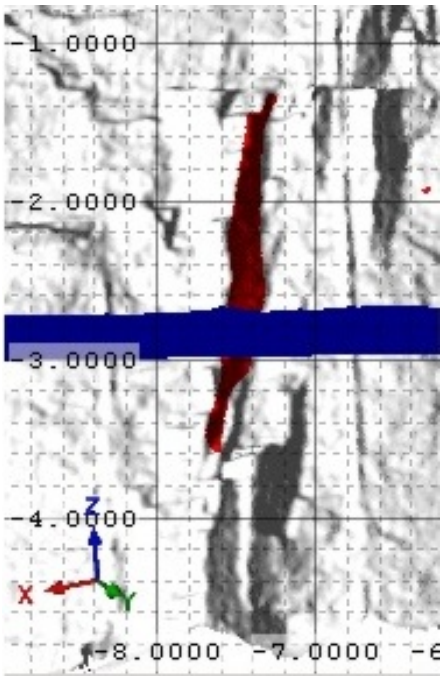

Figure 43

After creating a new polydata object out of the selected area (Figure 44a) the length of the discontinuity surface is measured with the command "measure distance" (Figure 44b).

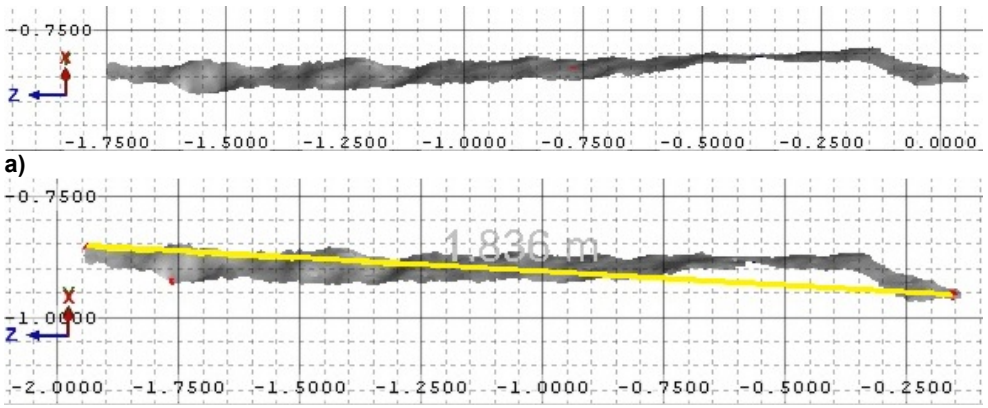

a)

b)

Figure 44

For estimation of the JRC the profile is then compared to Barton's roughness profiles for large scale or small scale depending on the length of the discontinuity surface (the profile above would be compared to large scale profiles) (Chapter 2.2.7).

3.6.5.2 Determination of Roughness after Palmström

All steps described above are also required for determination of roughness after Palmström. After measuring the length a plane is created out of the discontinuity surface (Figure 45).

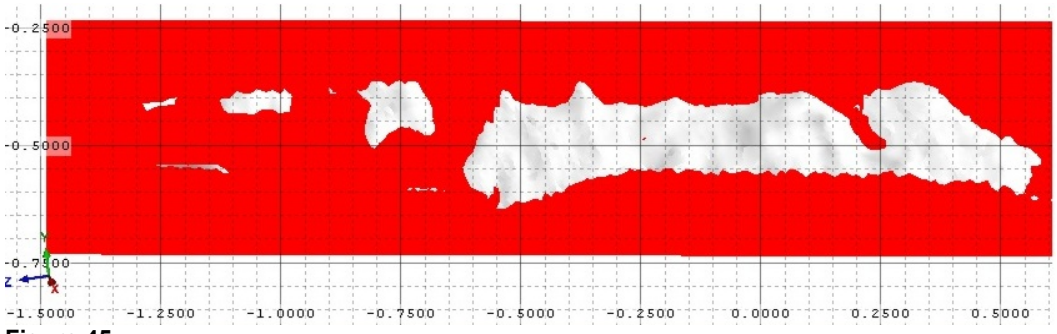

Figure 45

When opening an object RiSCAN PRO offers the option to select a view. Parameters that have to be selected for determination of the amplitude are marked by red circles in Figure 46a). The plane created out of the discontinuity surface must be chosen.

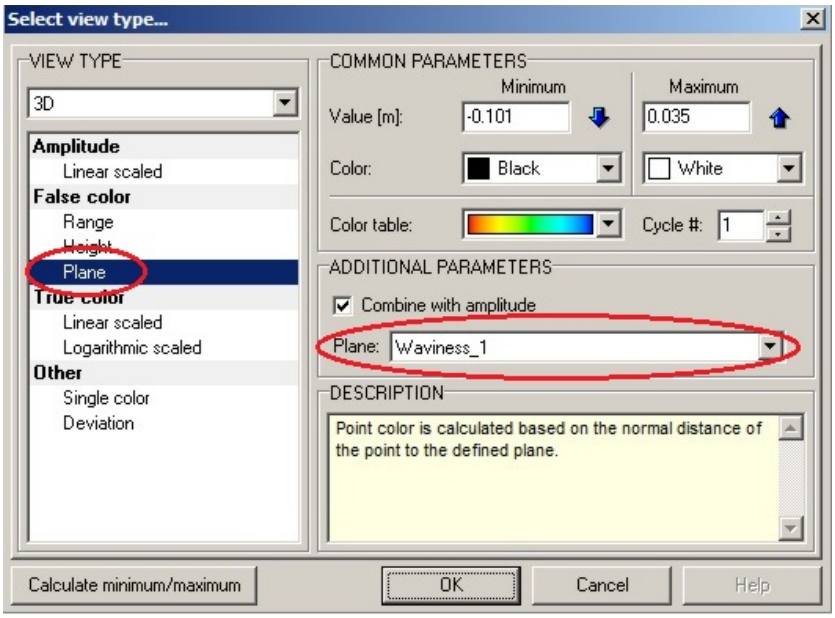

a)

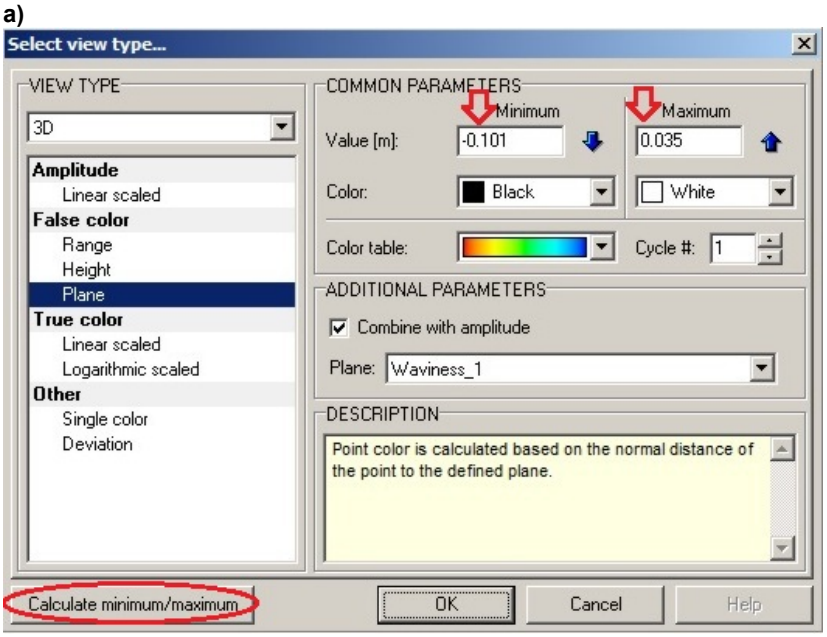

b)

Figure 46

The divergence of the discontinuity surface from the plane is then determined by calculating the minimum and maximum values (Figure 46b). The sum of these values determines the maximal amplitude.

As the length is already known the undulation and consequently the roughness can be determined applying the steps described in Chapter 2.2.7.

4 Results

4.1 Comparison of Registration Methods

Registration methods differ both in accuracy and time exposure regarding field and indoor work.

4.1.1 Standard Deviation

The accuracy of different registration methods introduced in Chapter 3.5.1 is reported here.
Figure 47 shows the standard deviation of each method for three different scan positions.

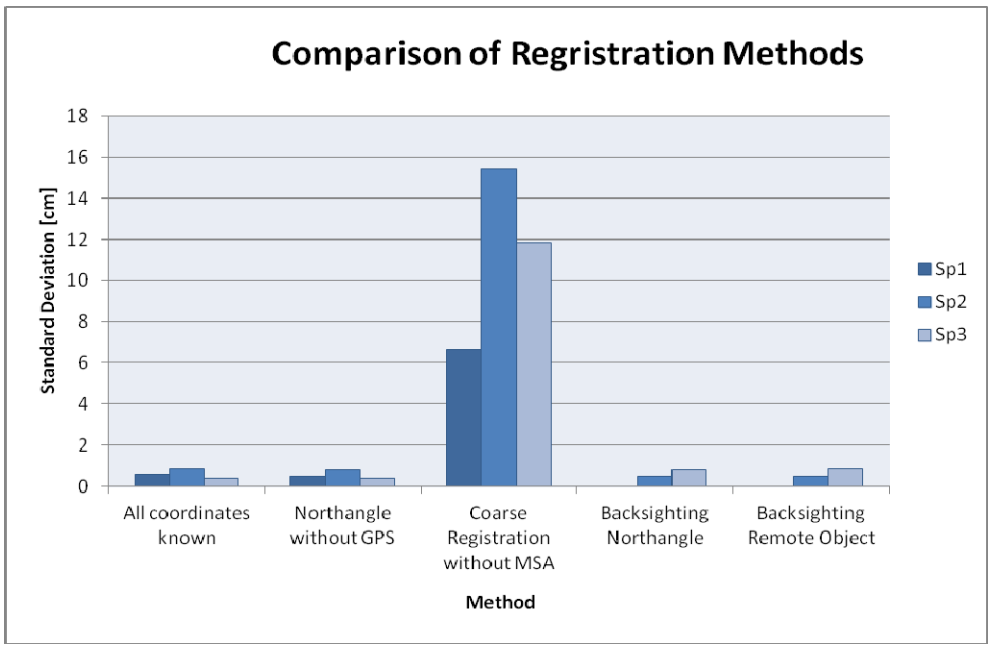

Figure 47: Comparison of standard deviations for different registration methods

Obviously the highest standard deviation (more than 10 cm) occurs under manual coarse registration. By running additionally a multi station

adjustment, the deviation gets reduced to 6.7 cm. No difference is showing between backsighting against north or a remote object.
Furthermore no significant difference between north angle registration without GPS coordinates and GPS registration with all coordinates is observable.
In general standard deviations of scan position 2 (Sp 2) are higher in three of five methods.

4.1.2 Time Exposure

Figure 48a) shows the estimated amount of time each method requires altogether and with regard to the outdoor and indoor effort (Figure 48b). It is important to mention that time needed for data acquisition was excluded and the estimations were made for three scan positions and six tie points. Figure 48a) shows that registration with all GPS coordinates known and coarse registration including MSA are most time consuming whereas backsighting methods require the least of time. “Outdoor” in Figure 48b) represents activities that needed to be done to apply the different methods i.e. measurement of the deflection from north, GPS measurements of the tie points or installation of tie points. “Indoor” means time required for registration in RiSCAN PRO. Differences between “outdoor” and “indoor” activities are only observable in methods that used GPS.

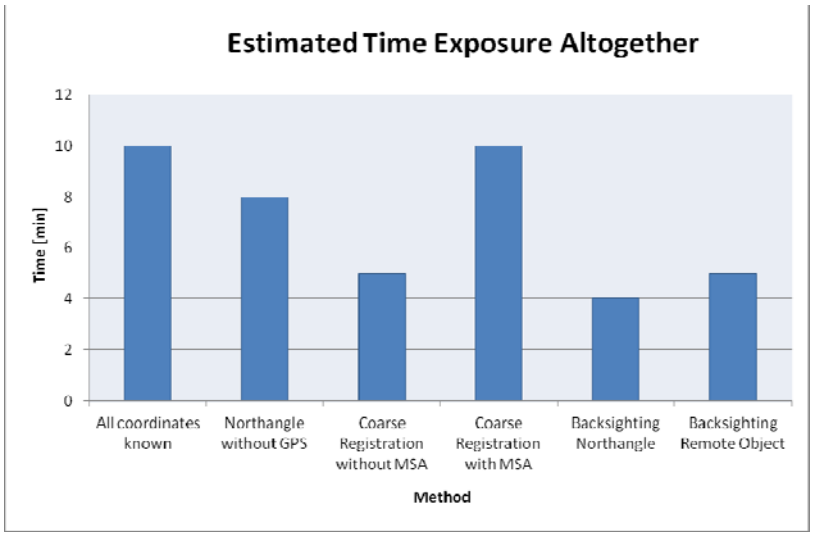

a)

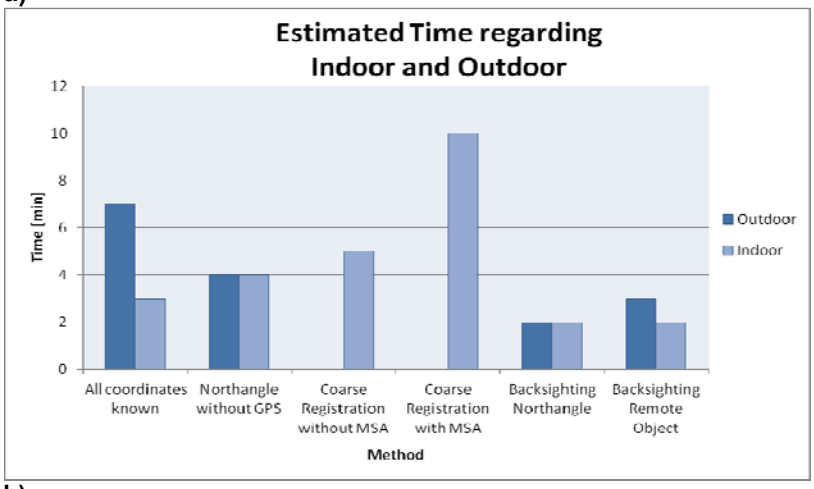

b)

Figure 48: Estimated time exposure altogether (a) and split to "Outdoor" and "Indoor" activities for three scan positions and six tie objects (b)

4.2 Angenofen

4.2.1 Rock Mass Characterization

A scanline survey with RiSCAN PRO was carried out on the middle wall of the quarry. Additionally to the method described in Chapter 3.6.2, orientation was also determined by manual measurements and

ShapeMetrix$^{3D.}$ To estimate the accuracy of the RiSCAN PRO-method it was compared to ShapeMetrix^{3D}.

4.2.1.1 Scanline Survey

The scanline was 19.28 m in length and covered the whole middle wall of the quarry. Along the line the data of 22 discontinuity planes could be collected due to rather wide spacing. It was attempted to collect all parameters that usually are also estimated in the field. However, for reasons that will be discussed in Chapter 4.4.2.2 only following parameters could be gathered:

- Orientation
- Spacing
- Frequency
- Block Size
- Trace Length
- Termination
- Roughness

4.2.1.1.1 Orientation

In the range of the scanline three joint sets could be determined that are plotted in Figure 49.

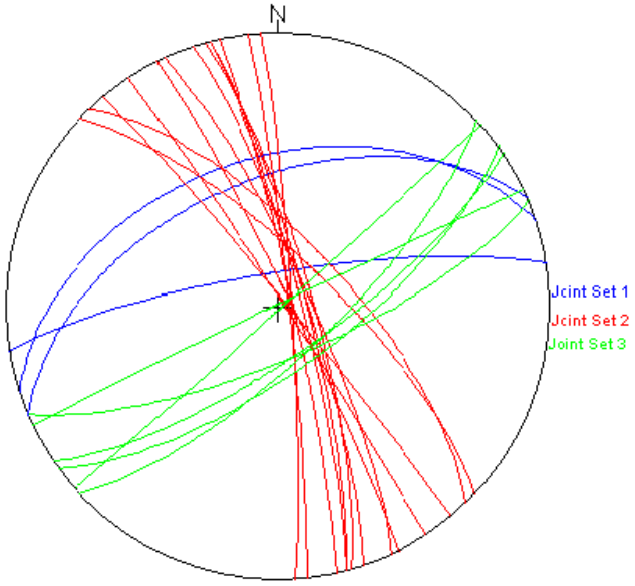

Figure 49: Great circles of the three joint sets plotted in a stereographic projection

Figure 50 shows the model of the middle wall with the extrapolated planes of three joint sets intersecting the scanline (blue).

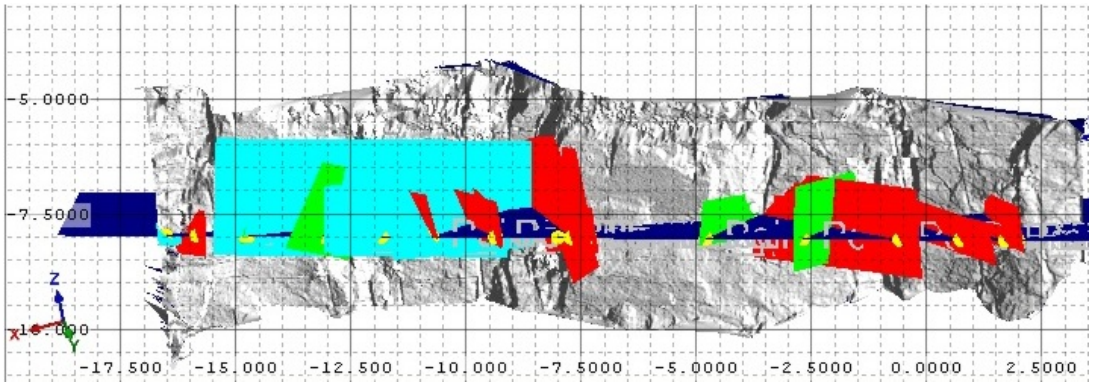

Figure 50: Model of the middle wall of Angenofen showing the scanline (dark blue), the intersection points (yellow), joint set 1 (light blue), joint set 2 (red) and joint set 3 (green)

4.2.1.1.2 Spacing

The true spacing, global and per set, is shown in Figures 51 and 52. It was classified after ISRM 1981 from extremely close spacing to extremely wide spacing.

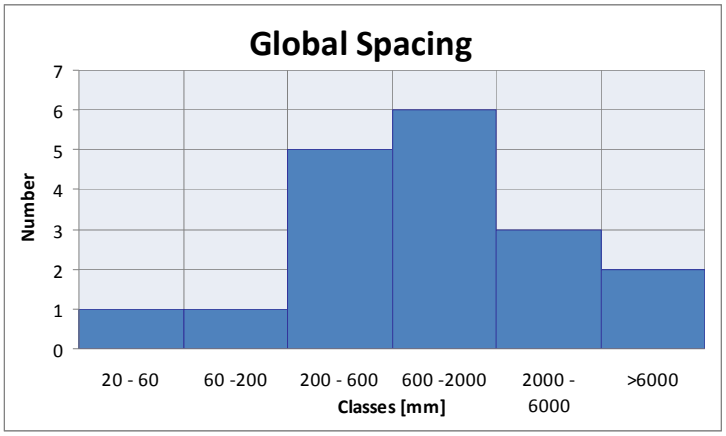

Figure 51: Global spacing in mm

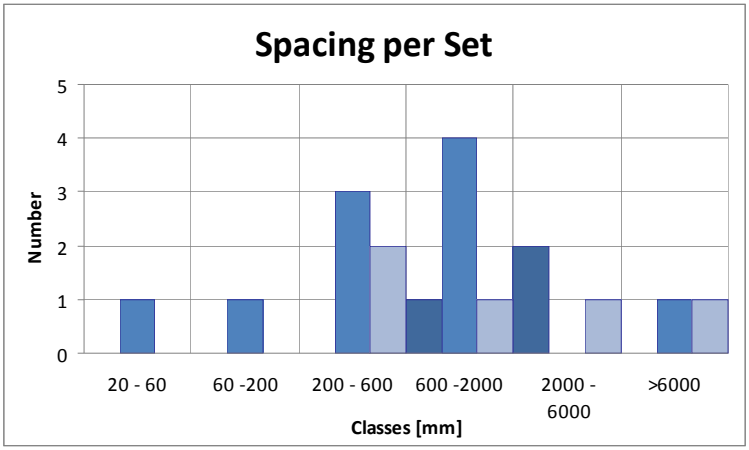

Figure 52: Spacing per set in mm (joint set 1: dark blue, joint set 2: middle blue, joint set 3: light blue)

Using the classification of Chapter 2.2.3 the outcrop consists of mainly moderate to very wide spaced discontinuities with only a few closed and extremely closed exceptions.

Figure 52 shows that discontinuities of joint set 1 are spaced wide to very wide, whereas joint set 3 consists of moderately spaced discontinuities. Joint set 2 plots from moderate to wide spacing. Only one joint of the set is in the extremely wide class.

4.2.1.1.3 Frequency

Frequency is the inverse value of true spacing and gives the number of discontinuities per unit. As shown in Figure 53 most discontinuities can be found within 0 to 0.75 m which reflects the spacing shown in Figure 51, where most discontinuities are located in the intervals up to 2000 mm.

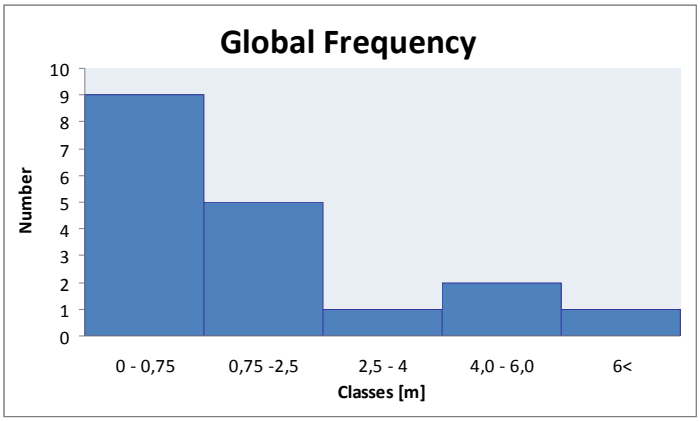

Figure 53: Global Frequency in m

4.2.1.1.4 Block Size

A volumetric joint count (J_v) (Chapter 2.2.5) was made for the first 10 meters of the scanline. 12 joints exist in this range, 3 belong to joint set 1, 5 to joint set 2 and 4 to joint set 3. Thus J_v is 1.2 / m³ which represents large blocks (after ISRM, 1981).

4.2.1.1.5 Trace Length

The trace length of most discontinuities shown in Figure 54 is smaller than 2.0 m. Only one trace of joint set 2 is larger than 3.25 m. Joint set 3 plots up to 2 m. Discontinuities of joint sets 1 and 2 mainly plot up to 2 m. 4 trace lengths of the two sets are larger than 2 m (Figure 55).

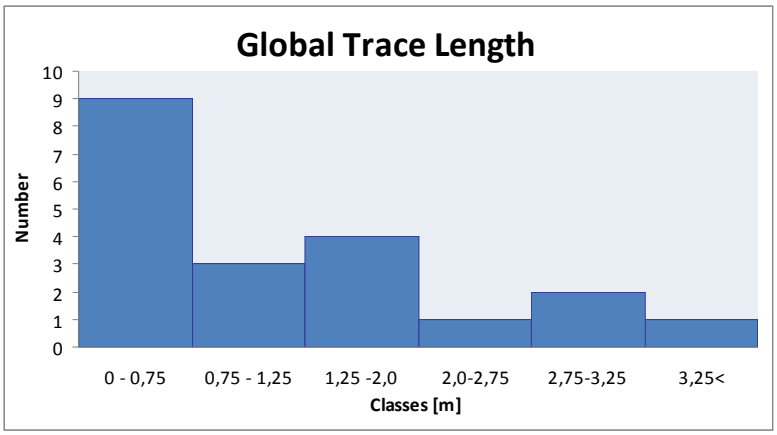

Figure 54: Global Trace Length in m

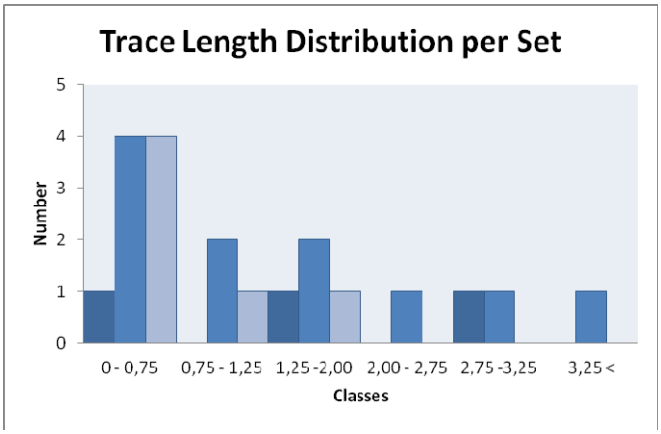

Figure 55: Trace length distribution per set in m (joint set 1: dark blue, joint set 2: middle blue, joint set 3: light blue)

4.2.1.1.6 Termination

In Figures 56 and 57 the termination for the trace length is shown global and per set for both ends of the trace. “R” represents traces ending in the intact rock, “D” shows the joints ending in another discontinuity and “X” marks the traces where no obvious end could be determined within the outcrop.

Figure 56 indicates that all ends except for one could clearly be defined to end in either intact rock or discontinuities.

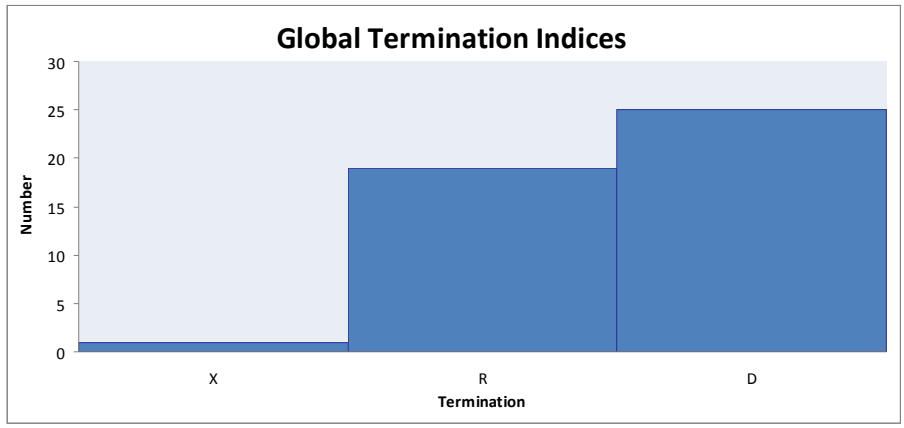

Figure 56: Global Termination Index for the middle wall

The Termination Index for global termination is 21 %.

The distribution in Figure 57 shows that joint set 1 and 2 blend in intact rock whereas endings in other discontinuities clearly dominate traces of joint set 3.

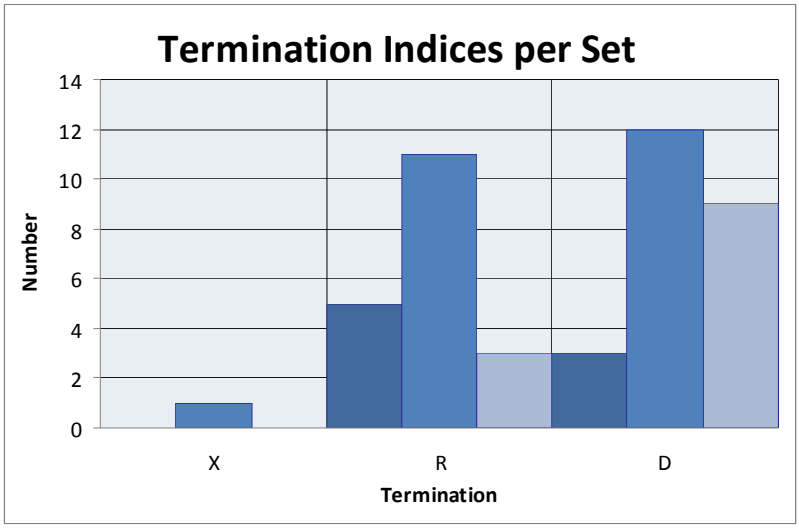

Figure 57: Termination distribution per set (joint set 1: dark blue, joint set 2: middle blue, joint set 3: light blue)

4.2.1.1.7 Smoothness and Waviness

Smoothness and waviness were determined by calculation of undulation (u) for each plane (Chapter 2.2.7). After comparison with Palmström's diagram (2001) the rock mass can be defined as strongly undulating and very rough because undulation is only for one plane smaller than 3 % (Table 6).

Discontinuities < 1m	u [%]	Discontinuities > 1m	u [%]
1	12	7	7
2	12	9	4
3	12	10	10
4	20	14	9
5	11	15	7
6	14	18	7
8	9	19	8
11	6	20	2
12	13		
16	11		
17	8		
21	4		
22	8		
23	16		

Table 6: Undulation of discontinuities bigger and smaller than 1 m in %

Figure 58 shows a typical profile for waviness in the outcrop.

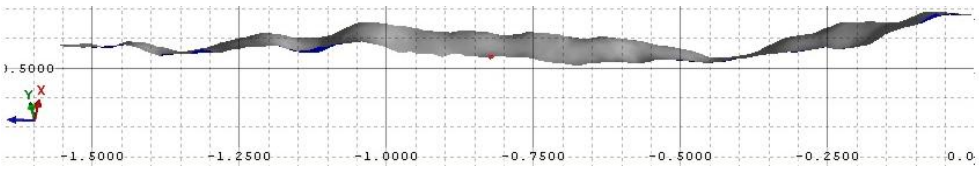

Figure 58: Waviness of the discontinuity surface intersecting the scanline at intersection point 7 which is 1.5 meters in length.

4.2.1.2 Orientation

Basically the orientation of the joint planes of the outcrop was measured using RiSCAN PRO. However, as the method is rather new, a more tested method, i.e. photogrammetry, was also applied and the results of both were then compared. Furthermore few compass measurements were taken manually for only one wall due to lack of time.

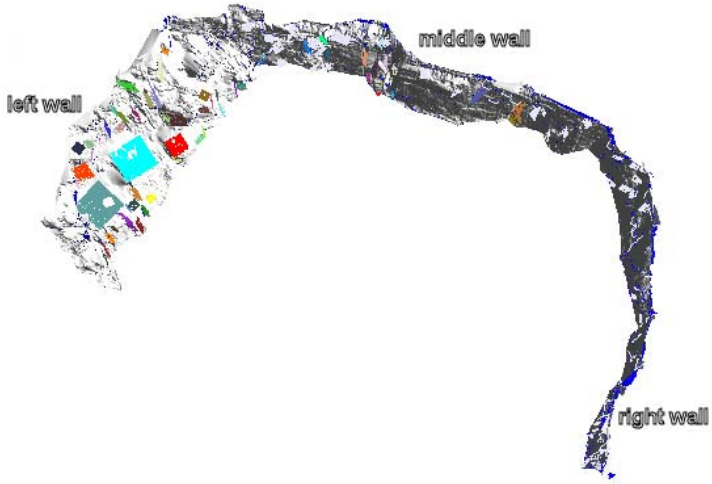

Figure 59: RiSCAN PRO model of the quarry in bird's view

All in all 150 planes were created in the U-shaped triangulated model of the quarry. For triangulation as well as for measurements the quarry was divided into three sections that will be referred to as left, middle and right

section of the outcrop (Figure 59). For each wall 50 planes were created out of selected joint plane areas.

Also photogrammetric models using ShapeMetrix^{3D} were generated. An example is shown in Figure 60.

For comparison of the values it was attempted to create planes and orientations out of exactly the same joint planes in both models.

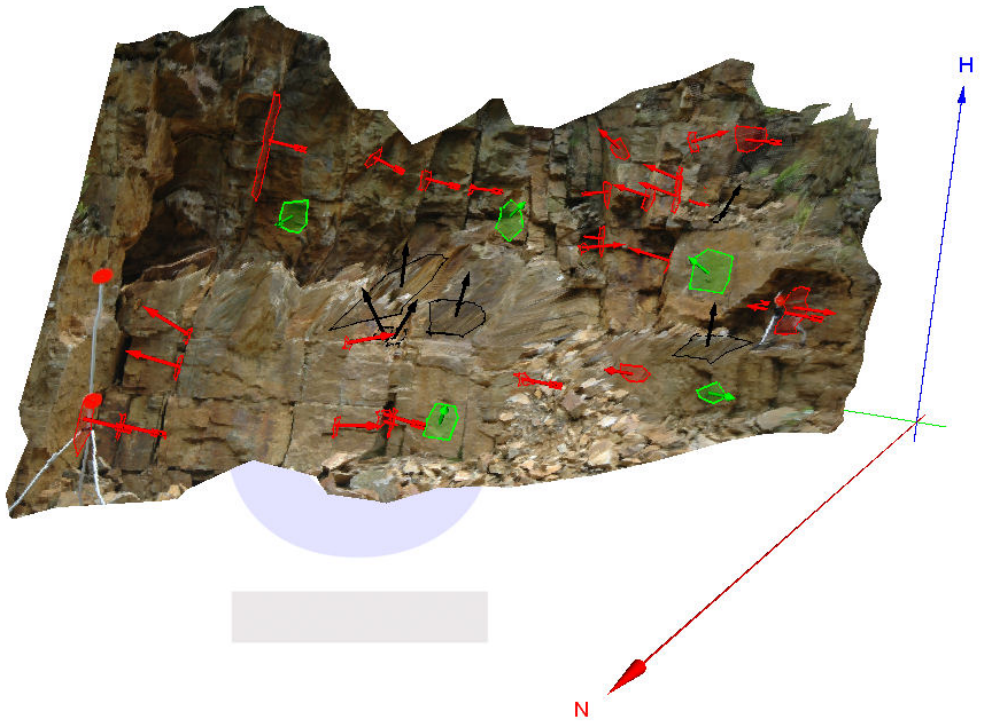

Figure 60: ShapeMetrix^{3D} model for the quarry's left wall

However, for reasons that will be discussed in Chapter 4.4.2.2, only 75 planes located in the left and middle section matched in both models and could be used for a statistical analysis. Figure 61 a) & b) show the stereonet projections of the two different approaches.

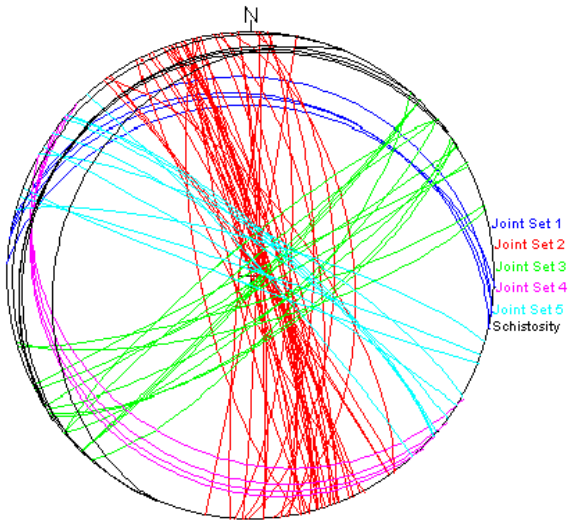

a)

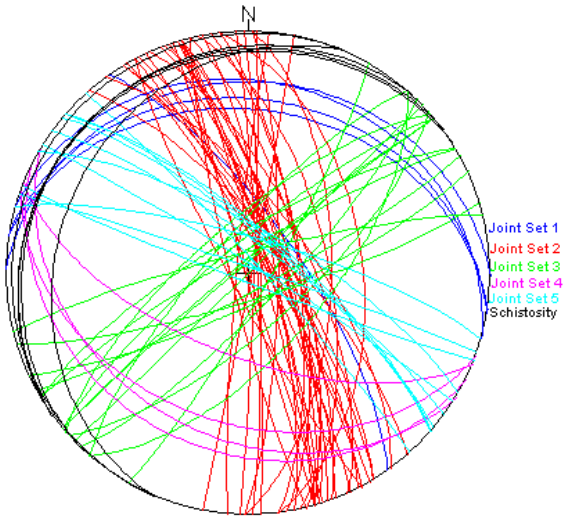

b)

Figure 61: Stereographic Projections for each method: a) RiSCAN PRO b) ShapeMetrix^{3D}

4.2.1.2.1 Comparison of the Orientation Measurements

For comparison of RiSCAN PRO with ShapeMetrix^{3D} the poles of each joint set were plotted for both methods (Figures 62 to 67).

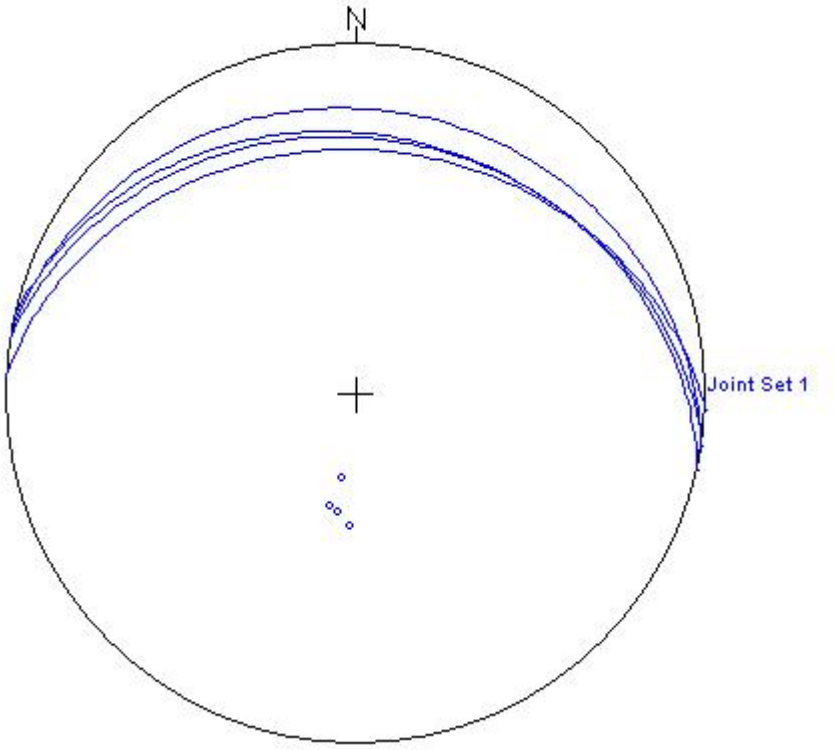

a)

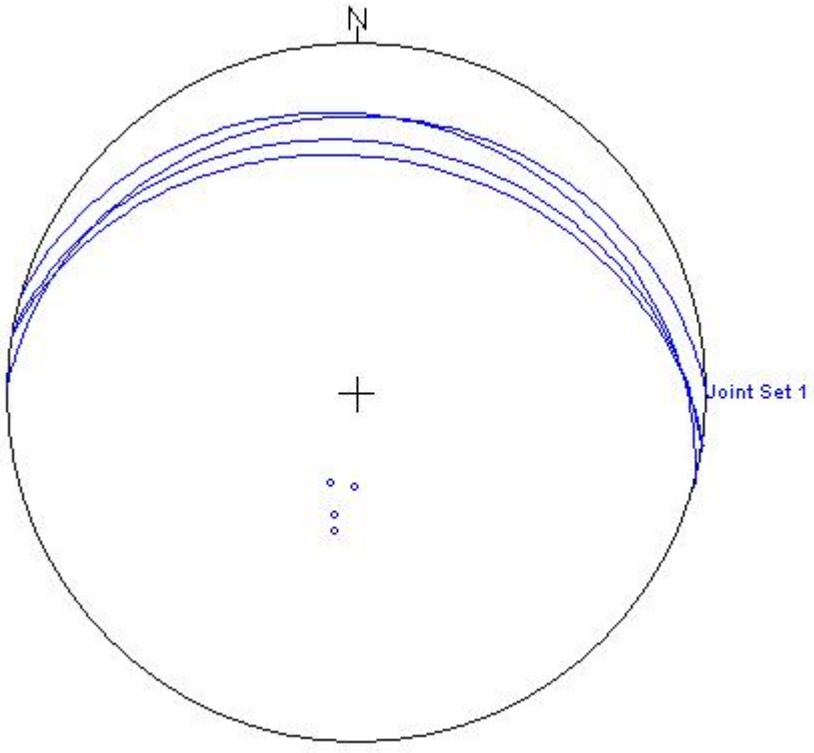

b)

Figure 62: Poles and great circles of joint set 1 for RiSCAN PRO (a) and ShapeMetrix^{3D} (b)

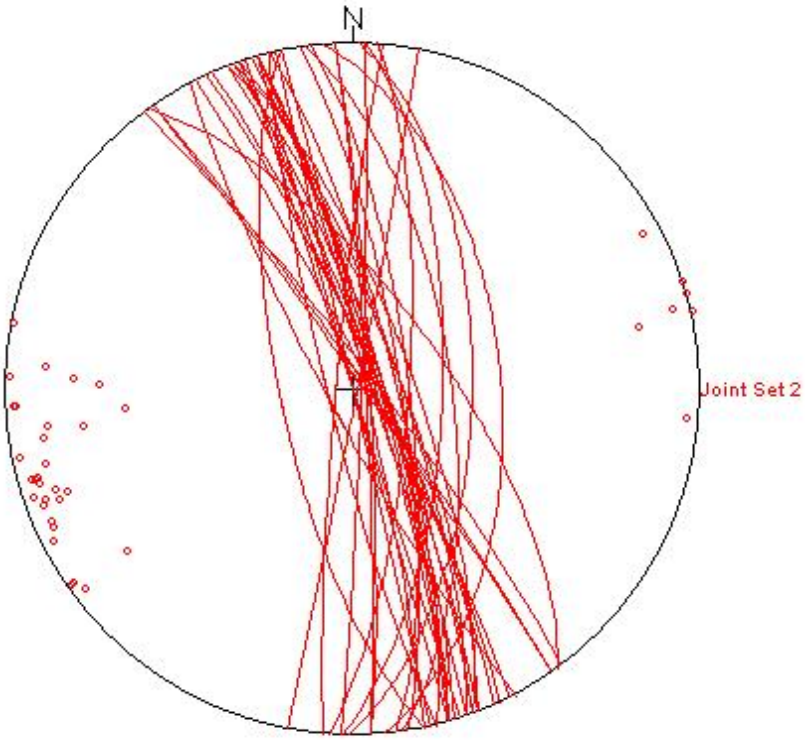

a)

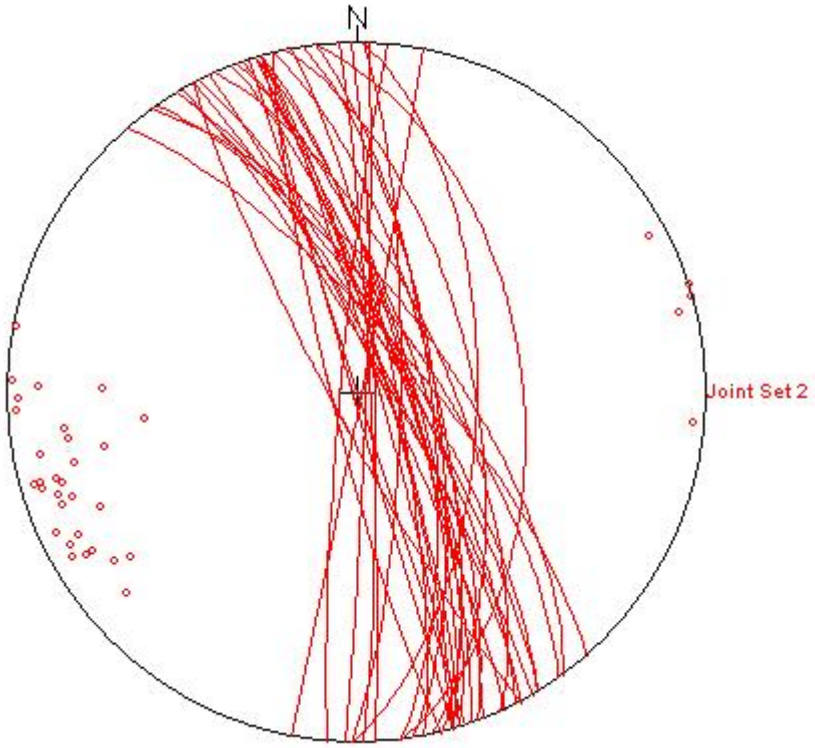

b)

Figure 63: Poles and great circles of joint set 2 for RiSCAN PRO (a) and ShapeMetrix^{3D} (b)

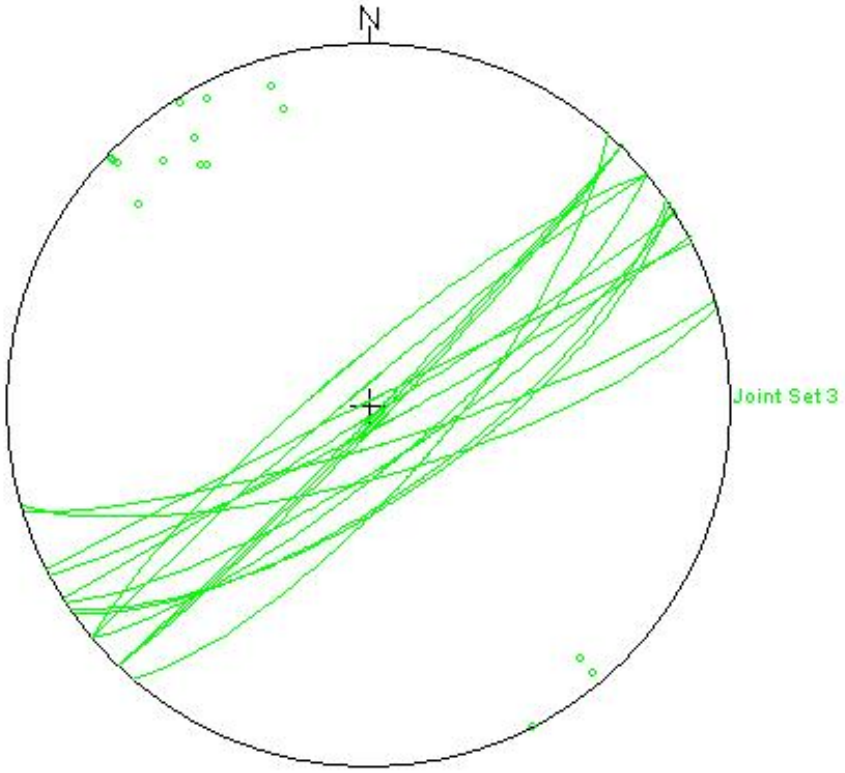

a)

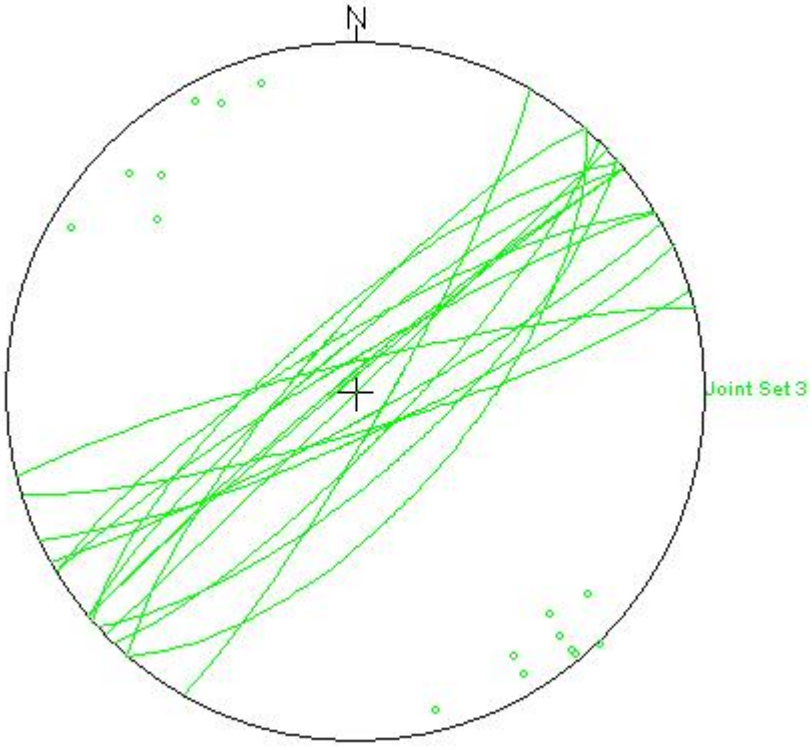

b)

Figure 64: Poles and great circles of joint set 3 for RiSCAN PRO (a) and ShapeMetrix^{3D} (b)

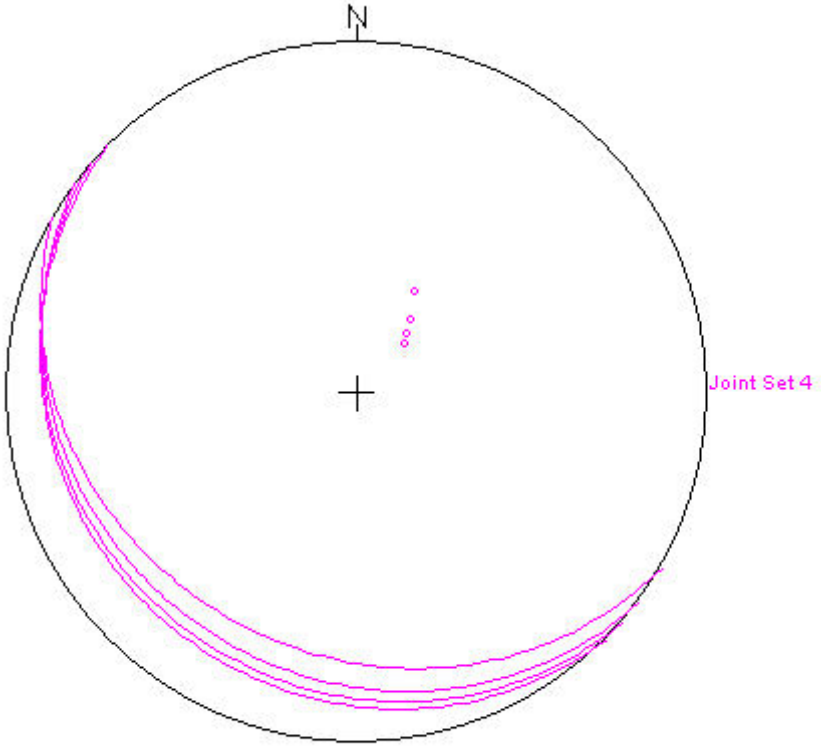

a)

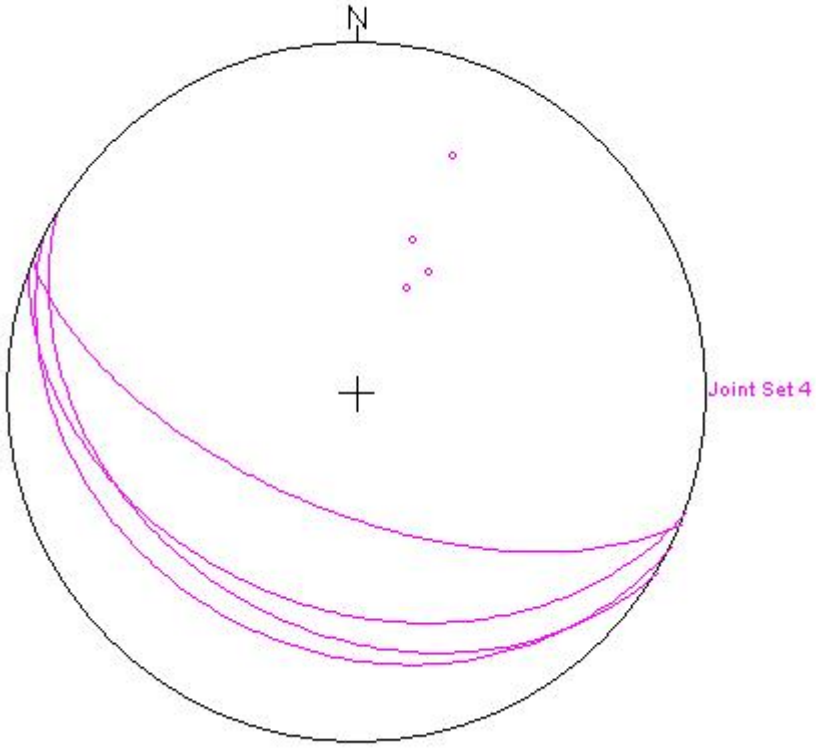

b)

Figure 65: Poles and great circles of joint set 4 for RiSCAN PRO (a) and ShapeMetrix^{3D} (b)

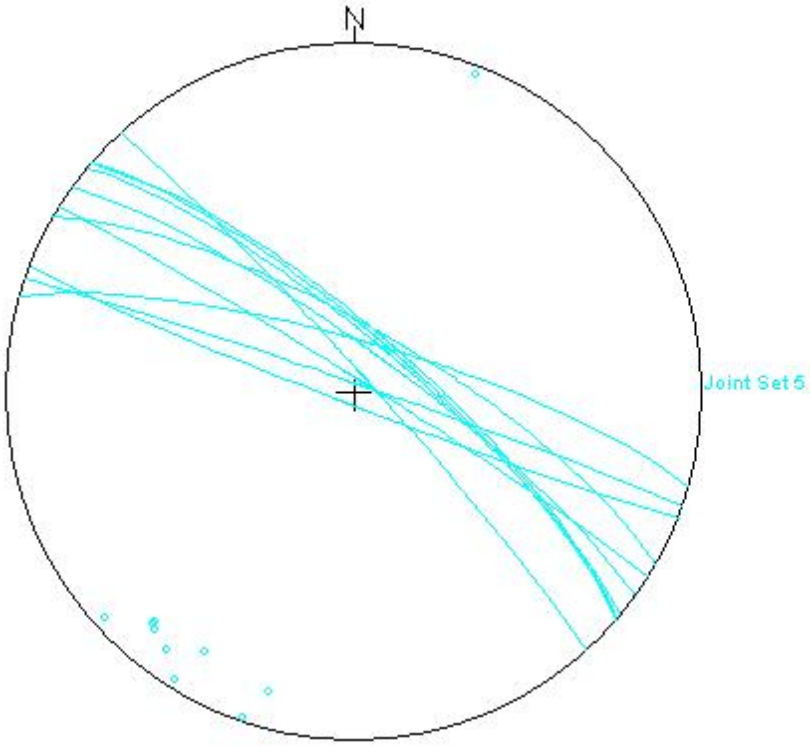

a)

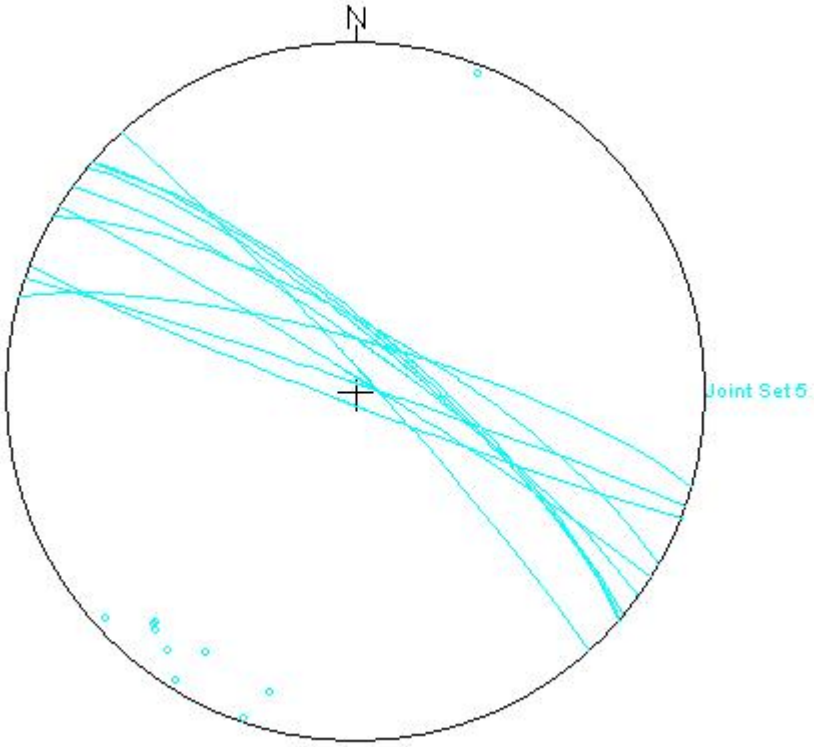

b)

Figure 66: Poles and great circles of joint set 5 for RiSCAN PRO (a) and ShapeMetrix^{3D} (b)

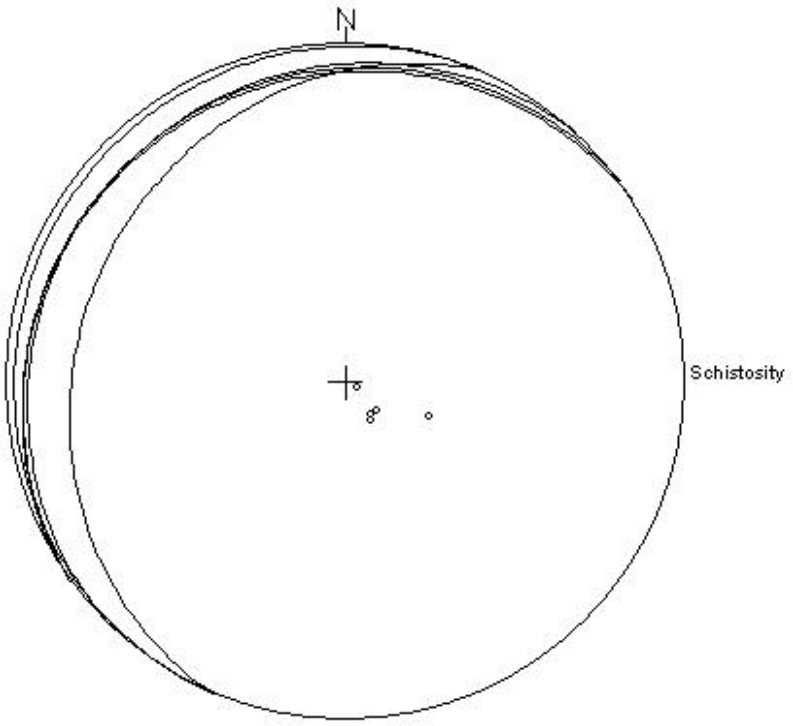

a)

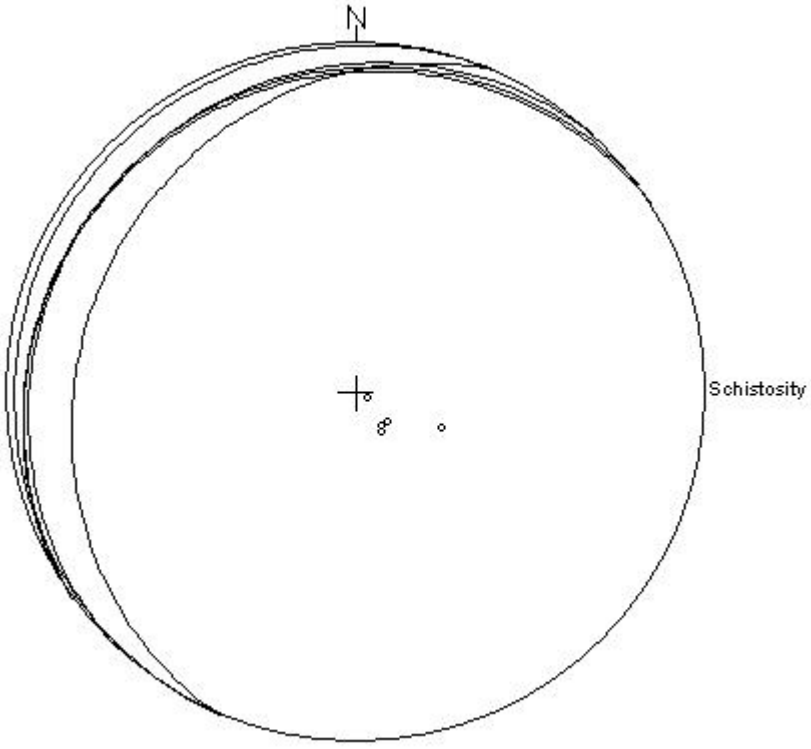

b)

Figure 67: Poles and great circles schistosity for RiSCAN PRO (a) and ShapeMetrix$^{3D(}$ (b)

Next, the centroid was calculated for each joint set and for the schistosity with Sphaira (Table 7).

	ShapeMetrix3D		RiSCAN Pro	
	Dip Direction	Dip Angle	Dip Direction	Dip Angle
JS 1	9	26	8	26
JS 2	75	81	74	85
JS 3	143	89	141	83
JS 4	205	33	217	20
JS 5	35	81	34	81
Schistosity	319	8	319	8

Table 7

In a last step the dihedral angle between RiSCAN centroid and ShapeMetrix^{3D} centroid, which belongs to the same set, was calculated (Table 8).

	Dihedral Angle
JS 1	0
JS2	4
JS 3	6
JS 4	14
JS 5	1
Schistosity	0

Table 8

As it can be seen in Table 9 there is no difference between the centroids of joint set 1 and the schistosity. Also the orientation differences of JS2, JS3 and JS5 are very low. The highest difference between the two methods is observable in joint set 4. The reasons for the high difference will be discussed in Chapter 4.2.2.2.

Additionally 7 compass measurements were compared to the results of the computer programs (Figures 68 and 69).

While planes 1 to 5 fit quite well (Figure 68), the RiSCAN PRO value of measurement number 6 has a significantly lower dip angle than the compass and ShapeMetrix^{3D} measurements. On the other hand plane 7 shows a low ShapeMetrix^{3D} value compared to RiSCAN PRO and the compass.

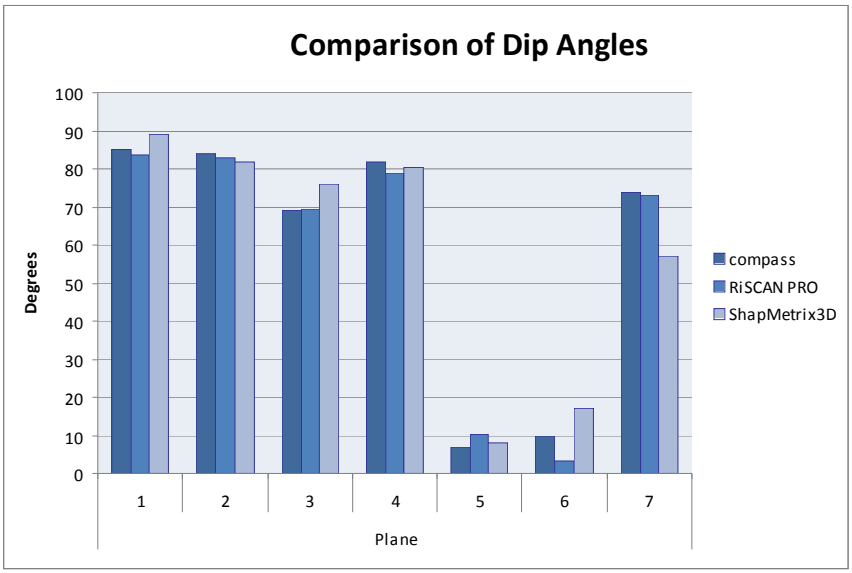

Figure 68

The diagram below indicates slightly higher ShapeMetrix^{3D} values for azimuths in planes 1, 2, 3, 4 and 7, whereas the compass data of measurements 5 and 6 are higher.

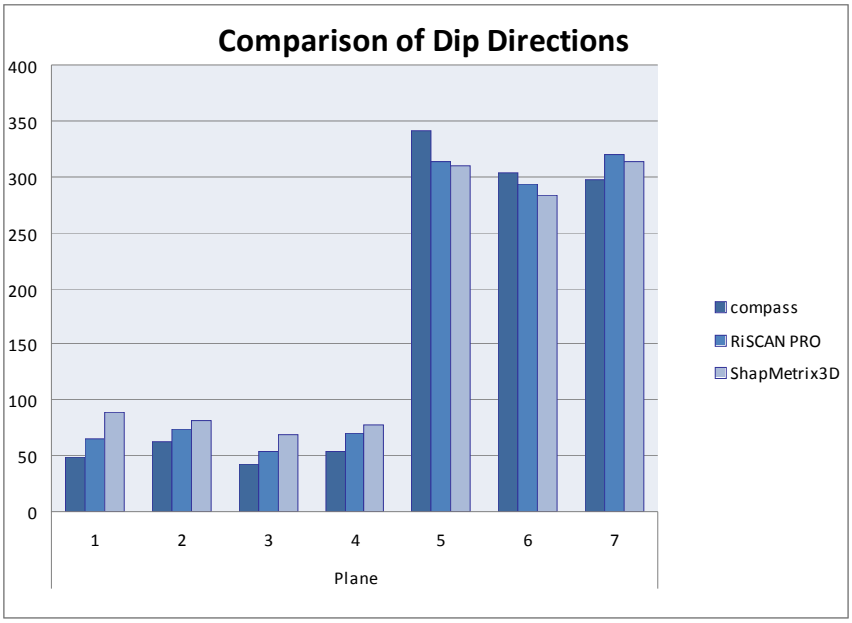

Figure 69

4.3 Arzberg

4.3.1 Orientation Measurements

For measurements of orientation it was assumed that the used computer program does not offer dip angle and dip directions for planes automatically but only coordinates of the plane's normal. Hence dip angle and dip direction were calculated with the method using direction cosines described in Chapter 3.6.2.2. Eleven values of manual measurements were compared to the results of the calculation with direction cosines. For comparison again the centroids and dihedral angles were calculated for both joint sets (Table 9).

	Compass		RiSCAN PRO	
	Dip Direction	Dip Angle	Dip Direction	Dip Angle
JS 1	207	36	212	38
JS 2	343	64	343	72

Table 9

In general RiSCAN PRO produces slightly higher values.

Table 10 shows the dihedral angle between the centroids of both methods.

	Dihedral Angle
JS 1	4
JS 2	8

Table 10

As shown in Figure 70 and 71 differences between dip angle values for single planes are larger than for dip directions.

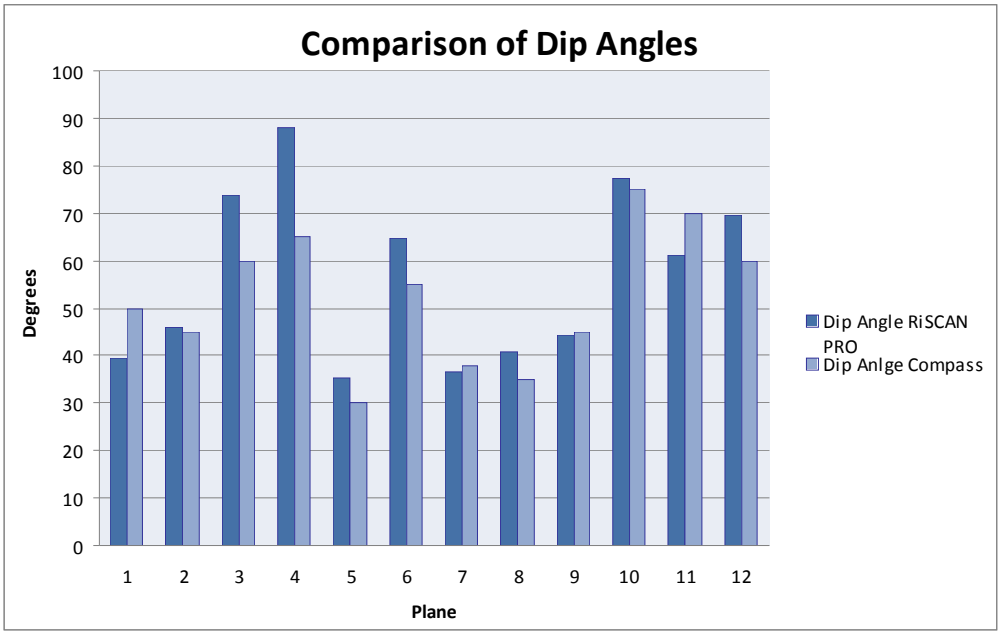

Figure 70: Comparison of dip angles

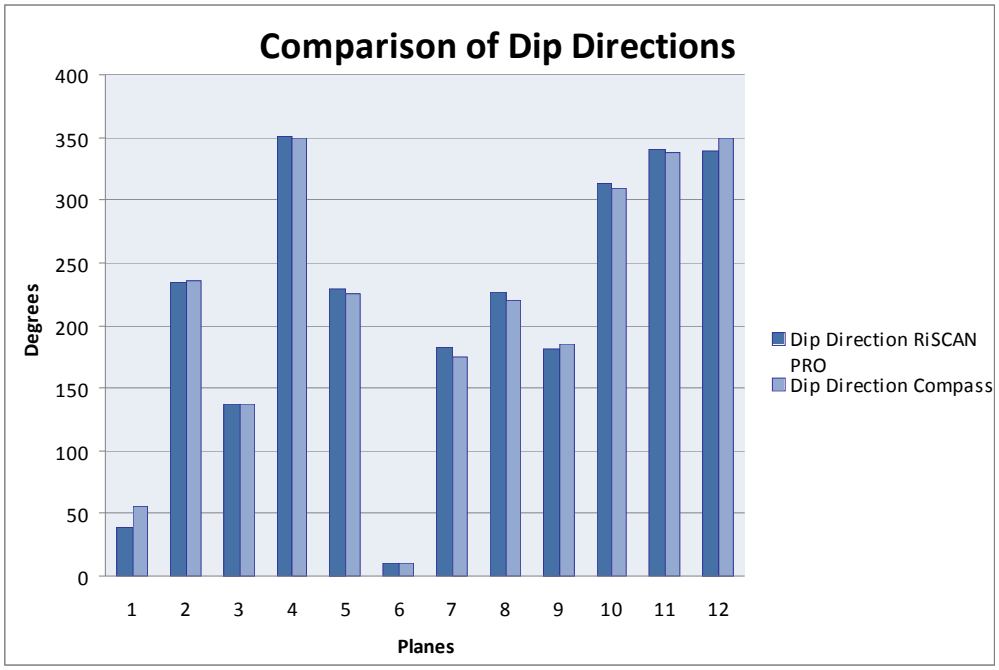

Figure 71: Comparison of dip directions

The stereonet in Figure 72 shows the poles of the eleven planes. RiSCAN PRO estimations and compass measurements for one plane are marked in the same color.

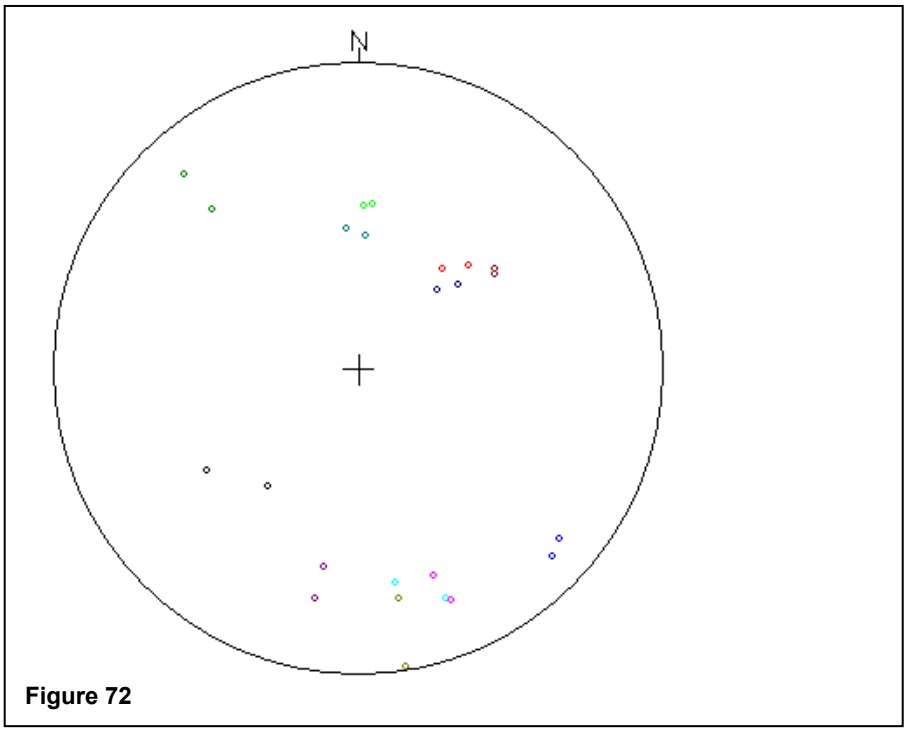

Figure 72

4.4 Discussion

4.4.1 Comparison of Registration Methods

Time exposure is of course dependent on the number of scan positions and tie objects. The time consumed for data acquisition and accuracy of GPS coordinates varies with the GPS reception which is dependent on location and weather.

Basically it is up to the scan provider which method is used for registration. But under consideration of the required accuracy, the available time and the GPS reception, a recommendation can be made for application in engineering geology.

If possible a RTK- GPS should be used to specify the location. However, considering that in most projects the highest accuracy should be achieved within shortest period of time, backsighting against a remote object or against north are most recommended for geology's purposes.

If no RTK-GPS is available also backsighting against north without global coordinates can be accomplished since important parameters to be determined in an engineering geological investigation do not absolutely require global coordinates.

4.4.2 Angenofen

4.4.2.1 Scanline Survey

The survey with RiSCAN PRO covers mainly geometric parameters. Further features, normally to be determined in the field, cannot be estimated on basis of a 3D-model. These are:

- Friction Angle
- UCS
- Filling

- Wetness

However, the scan providers could easily collect these parameters while the scan is carried out.
If the outcrop is not accessible some of the parameters as mentioned above could be derived from photos.
Palmström's and Barton's methods could be applied to RiSCAN PRO models.

4.4.2.2 Orientation

While on the left and middle wall of the outcrop nearly all planes of the RiSCAN PRO model could be matched with the ShapeMetrix^{3D} model, on the right wall only 11 planes could be found in both models. This can be explained by the different sections of the right wall both models were created out of. Furthermore some joint planes were too small for accurate mapping in ShapeMetrix^{3D}. It was difficult to create exactly the same planes in both models. That might be the reason for the high dihedral angle of joint set 4. Differences of the compass measurements and the estimations of two programs occur due to the fact that with a compass only the field of the bearing area is measured, which is usually a very small part compared to the whole joint plane, whereas the selected areas in the programs are bigger and an average orientation of all points in the selection is calculated more reliably.
Lower dip angles in RiSCAN PRO (plane 6 in Figure 68) are the result of elimination of shadow zones, where only few or no data could be acquired. For modeling shadow zones holes are closed by interpolation. Thus curvature has no influence on the resulting planes and the dip angle is not as steep as in reality. ShapeMetrix^{3D} interpreted an extremely high dip angle of plane 6 in Figure 68.
Altogether the results of orientation measurements with RiSCAN PRO are similar to the compass measurements and to the values measured

with the already tested ShapeMetrix^{3D}. This implies that RiSCAN PRO can be applied for measuring orientations of fracture planes.

4.4.3 Arzberg

The gallery was very narrow which caused some difficulties. During data acquisition three people were in the tunnel, two of them had to wait in the recesses of “Nordschalg” and “Raabschacht” to avoid further ghost points. Only one person could stay at the scanner.
The model could not be colored as many pictures taken were blurred due to the closeness to the wall. It was very difficult to re-locate exactly the manually measured planes in the LiDAR model. This might be the main reason for the high differences in the dip angle values of compass measurements and estimations of RiSCAN PRO shown Figure 71. Furthermore in the present LiDAR model it was hard to distinguish between natural discontinuities and damages caused by excavation.

5 Conclusion

Data acquisition with a terrestrial laser scanner and post processing with RiSCAN PRO produce photo-realistic georeferenced models of the scanned area.

Determination of parameters for rock mass characterization was based on methods that are also applied in the field. Regarding orientation the RiSCAN PRO results were compared to the more proven method of photogrammetry using ShapeMetrix^{3D} and it showed that the results for dip angle and dip direction are essentially the same.

Also with RiSCAN PRO it was attempted to determine as many parameters as usually are recorded along a scanline in the field. However, with LiDAR models only parameters based on geometric functions can be acquired. A virtual scanline survey, accomplished in a part of the quarry of Angenofen, showed that discontinuity characterization can be applied by combining the measurements of RiSCAN PRO with traditional analysis methods.

Other parameters like weathering stage and wetness could be estimated from the photos that were recorded after the scan, if the scan position was not too far away from the outcrop.

In the underground LiDAR survey orientations were only compared to compass measurements. The results were satisfying, but a method for the differentiation between natural discontinuities and damaged planes in a LiDAR model should be a further research topic.

As a conclusion it can be stated that the models made with RiSCAN PRO are detailed reproductions of the nature outcrops. Since the most important parameters for discontinuity characterization can also be determined using the program, laser scanner data sets processed with RiSCAN PRO are applicable for engineering geology.

Development of terrestrial laser scanning in the future should focus on how to improve the speed of scanning without losing resolution so that terrestrial laser scanners can also be applied in current tunnel excavation projects to record, for example the heading face.

6 Bibliography

3G SOFTWARE&MEASUREMENT GmbH (2006): ShapeMetrix^{3D} 3D imaging for measuring and assessing rock and terrain surfaces, User Manual for Version 1.9, p.2-1 to 2-3

ABELLÁN, A., VILAPLANA, J.M., MARTÍNEZ, J. (2006): Application of a long-range Terrestrial Laser Scanner to a detailed rockfall study at Vall de Núria (Eastern Pyrenees, Spain). Engineering Geology, 88, p.136-148

BITELLI, G., DUBBINI, M., ZANUTTA, A. (2004): Terrestrial Laser Scanning And Digital Photogrammetry Techniques To Monitor Landslide Bodies. XXth ISPRS Congress: Proceedings of Commission V, Istanbul, Turkey, p. 246-251

BUCKLEY, J. Simon, HOWELL, A., ENGE, D.H., KURZ, H.T.(2008) : Terrestrial laser scanning in geology: data acquisition, processing and accuracy considerations. Journal of the Geological Society, London, Vol. 165 pp. 625-638

FAUPL, Peter (2003): Historische Geologie. Facultas Verlags- und Buchhandels AG, Wien, p. 77 and 78

GOODMAN E. Richard & SHI Gen-hua (1985): Block Theory And Its Application to Rock Engineering. Prentice-Hall International, Inc. p. 26/27

ISRM (1981): Rock Characterization Testing & Monitoring ISRM Suggested Methods. Pergamon Press, Oxford, p. 5-46

KEMENY, J. & TURNER, K. (2008): Ground Based LiDAR Rock Slope Mapping and Assessment. Central Federal Lands Highway Division, p. 1-10 and p. 44

LIU, Q. & KIEFFER, S.D. (2011): Virtual Outcrop Modeling for 3D Characterization of Engineering Rock Masses. ARMA 11-425.

LIU, Q. & KIEFFER, S.D. (2012, accepted): Digital tunnel mapping using terrestrial LiDAR - a case study. International Symposium Rock Engineering &Technology for Sustainable Unterground Construction. Stockholm.

PALMSTRÖM, A. (2001): In-Situ Characterization of rocks. Lise/Abingdon/Exton(Pa), Tokio. p. 27-33

PRIEST, D. Stephen (1993): Discontinuity Anaylsis for Rock Engineering. Chapman&Hall, London.

RIEGL LMS GmbH (2009): Operating & Processing Software RiSCAN PRO for RIEGL 3D Laser Scanners, Version 1.5.2sp2.

SCHWALBE, E., MAAS, H-G., DIETRICH, R., EWERT, H. (2004): Glacier Velocity Determination From Multi Temporal Terrestrial Long Range Laser Scanner Point Clouds. XXth ISPRS Congress: Proceedings of Commission V, Istanbul, Turkey, p.457-462

SLOB, Siefko (2010): Automated rock mass characterisation using 3-D terrestrial laser scanning. Wöhrmann Print Service, Zutphen, p. 60-62 and 100-103

STURZENEGGER, M. & STEAD, D. (2009): Colos-range terrestrial digital photogrammetry and terrestrial laser scanning discontinuity characterization on rock cuts. Engineering Geology, 106, p.163-182

WARNER, A. Timothy, NELLIS, Duane M, FOODY, M. Giles (Editors) (2009): The SAGE Handbook of Remote Sensing. SAGE, p.199-211

WEBER,Leopold (2005): The Argentiferous Lead-zinc Mineralization of Arzberg (Eastern Styria). Joannea Geol.Paläont., 7, p. 9-23

Links:

Link 1 (8.3.2012):
http://www.spatialresources.com/id71.html
Link 2 (8.3.2012):
http://www.riegl.com/nc/products/terrestrial-scanning/
Link 3 (8.3.2012):
http://www.riegl.com/media-events/single-news/article/riegl-lms-z420i-monitoring-the-wreck-of-costa-concordia/
Link4 (8.3.2012):
http://portal.tugraz.at/portal/page/portal/Files/i2210/files/eng_geol/Riegl_LMS_Z620.pdf
Link 5 (9.03.2012):
http://www.riegl.com/uploads/tx_pxpriegldownloads/10_DataSheet_ManualTilt_07-2005_22-08-2006.pdf
Link 6 (07.03.2012) :
http://www.riegl.com/uploads/tx_pxpriegldownloads/10_DataSheet_Reflector-Targets_22-08-2006.pdf